

Dynamic Hubbard model: kinetic energy driven charge expulsion, charge inhomogeneity, hole superconductivity, and Meissner effect

J. E. Hirsch

Department of Physics, University of California, San Diego
La Jolla, CA 92093-0319

(Dated: February 19, 2013)

Dynamic Hubbard models are extensions of the conventional Hubbard model that take into account the fact that atomic orbitals expand upon double occupancy. These models give rise to superconductivity driven by lowering of kinetic energy when the electronic energy band is almost full, with higher transition temperatures resulting when the ions are negatively charged. It is shown here that systems described by dynamic Hubbard models have a tendency to expel negative charge from their interior to the surface, and they have a tendency to develop charge inhomogeneity in the bulk. These tendencies are largest in the parameter regime where the models give rise to highest superconducting transition temperatures. We propose this physics as an explanation for the charge inhomogeneity, negatively charged grain boundaries and negatively charged vortices observed in high temperature superconductors. Below the superconducting transition temperature the models considered here describe a negatively charged superfluid and positively charged quasiparticles, unlike the situation in conventional BCS superconductors where quasiparticles are charge neutral on average. We examine the temperature dependence of the superfluid and quasiparticle charges and conclude that spontaneous electric fields should be observable in the interior and in the vicinity of superconducting materials described by these models at sufficiently low temperatures. We furthermore suggest that the dynamics of the negatively charged superfluid and positively charged quasiparticles in dynamic Hubbard models can provide an explanation for the Meissner effect observed in those superconducting materials that are not described by conventional BCS-London theory.

PACS numbers:

I. INTRODUCTION

The conventional single band Hubbard model with Hamiltonian[1, 2]

$$H = - \sum_{i,j,\sigma} [t_{ij} c_{i\sigma}^\dagger c_{j\sigma} + h.c.] + U \sum_i n_{i\uparrow} n_{i\downarrow} \quad (1)$$

has been used to describe the physics of many real materials. The model ignores the fact that non-degenerate atomic orbitals are necessarily modified by double electronic occupancy[3–7]. To remedy this deficiency a variety of new Hamiltonians have been proposed and studied that we will generically call ‘dynamic Hubbard models’, that take into account the fact that *orbital expansion* takes place when a non-degenerate atomic orbital is doubly occupied[8–20].

One (of several[21]) ways to incorporate this physics is by the substitution[11, 22, 23]

$$U n_{i\uparrow} n_{i\downarrow} \rightarrow (U + \alpha q_i) n_{i\uparrow} n_{i\downarrow} \quad (2)$$

where α is a coupling constant (assumed positive) and q_i a local boson degree of freedom describing the orbital relaxation, with equilibrium position at $q_i = 0$ if zero or one electrons are present: upon double occupancy of the orbital at site i , q_i will change from zero to a negative value to reduce the electronic on-site repulsion, to an extent determined by the boson dynamics. If we describe the dynamics of this boson by a simple harmonic

oscillator[22]

$$H_i = \frac{p_i^2}{2m} + \frac{1}{2} K q_i^2 + (U + \alpha q_i) n_{i\uparrow} n_{i\downarrow} \quad (3)$$

the on-site repulsion is reduced from U to $U_{eff} = U - \alpha^2/(2K)$ when q_i takes the value $q_i = -\alpha/K$ corresponding to minimum energy when the site is doubly occupied, versus $q_i = 0$ when the site is unoccupied or singly occupied. The conventional Hubbard model does not allow the orbital to relax, in other words it corresponds to the limit $K \rightarrow \infty$ of an infinitely stiff orbital.

The Hamiltonian Eq. (3) breaks electron-hole symmetry[11]: the importance of this physics increases as the filling of the electronic energy band increases, as is simply seen by taking the mean field expectation value of Eq. (3). In addition, the importance of this physics increases when the ionic charge is small[11], since in that case the orbital expansion is larger (for example, the orbital expansion is larger for H^- than for He), corresponding to a smaller stiffness parameter K in Eq. (3). These two facts imply that the importance of this physics increases the more *negative charge* the system has. Thus, it will come as no surprise that a system where this physics is important will have a strong tendency to *expel negative charge*[24, 25]. This expulsion occurs already at the atomic level of course since the orbital expansion upon double occupancy implies radially outward motion of negative charge.

When an atomic orbital expands, the electronic kinetic energy is lowered, since in an orbital of radial extent r the electron kinetic energy is of order $\hbar^2/(2m_e r^2)$, with

m_e the electron mass. Thus, a system described by a dynamic Hubbard model will have lower electronic kinetic energy than if the orbital relaxation effect didn't happen. Just like at the atomic level the orbital expansion and associated negative charge expulsion is associated with lowering of kinetic energy, we will find for the system as a whole described by a dynamic Hubbard model that negative charge expulsion is associated with lowering of kinetic energy. Note however that our site Hamiltonian Eq. (3), describing orbital expansion when the value of q_i is negative, does *not* have a term explicitly describing the kinetic energy lowering of the atomic electron when q_i adopts a negative value.

There have been theoretical suggestions in the literature that electronic kinetic energy lowering may provide an unconventional mechanism for superconductivity[10, 26–43], applicable to materials that are not described by the conventional BCS-London theory that predicts an *increase* in kinetic energy upon the transition to superconductivity[44]. There have also been experimental indications that in certain materials and doping regimes the transition to superconductivity may be associated with kinetic energy lowering[45–54]. Since dynamic Hubbard models describe kinetic energy lowering a natural question is whether these models can describe superconductivity in cases where superconductivity is associated with lowering of kinetic energy. This is indeed the case[55–58].

In addition, dynamic Hubbard models are by nature electron-hole asymmetric and so are superconductors, as evidenced by the fact that a rotating superconductor develops a magnetic field that is always *parallel*, never antiparallel, to the direction of the mechanical angular momentum of the body[59]. This suggests that dynamic Hubbard models may be more appropriate to describe superconductors than the conventional Hubbard model that is electron-hole symmetric.

As a consequence of the charge expulsion physics the superconducting state in systems described by dynamic Hubbard models has quasiparticles that are *positively* charged on average[60], and as a consequence the superfluid has excess *negative* charge, in contrast to conventional BCS-London superconductors where quasiparticles are charge neutral on average. We will examine the consequences of this physics for superconductors described by these models at temperatures well below the superconducting transition temperature.

The potential (Coulomb) energy of a system of charges is minimized when the charge distribution is uniform. A non-uniform charge distribution gives rise to electrostatic fields and an associated potential energy cost. It will be favored if this cost is compensated by a kinetic energy gain, i.e. lowering of kinetic energy. Thus it is natural to expect, as we will find in this paper, that dynamic Hubbard models are prone to develop charge inhomogeneity, and in extreme cases charge separation, where the kinetic energy lowering overcompensates for the potential energy cost. Many materials of recent interest, in-

cluding high T_c cuprates and manganites, exhibit charge inhomogeneity[61–65], suggesting that dynamic Hubbard models may be useful to describe them.

In superconductors described by the conventional BCS-London theory, no negative charge expulsion occurs, the kinetic energy is raised rather than lowered in the transition to superconductivity, quasiparticles are charge neutral on average, and the Meissner effect is argued to be completely understood within the framework of the conventional theory[66–76]. In this paper we do not attempt to describe superconductors described by the conventional theory by dynamic Hubbard models. Rather, our aim is to describe superconductors that are *not* described by conventional BCS-London theory. There is general agreement among workers in the field that there are several classes of superconducting materials that are not described by conventional theory[77, 78]. All those materials exhibit a Meissner effect, and as mentioned there is experimental evidence for at least some unconventional materials that the kinetic energy is lowered in the transition to superconductivity. Since those materials are not described by the conventional theory it is certainly not obvious that the explanation of the Meissner effect of conventional superconductors provided by the conventional theory[66–76] would apply to these non-conventional materials. The negative charge expulsion physics driven by kinetic energy lowering of dynamic Hubbard models provides a natural explanation for the Meissner effect observed in these unconventional materials[79, 80]: just like in classical plasmas obeying Alfvén's theorem[81], the magnetic field lines move with the expelled negative charge.

II. DYNAMIC HUBBARD MODELS

Figure 1 depicts the essential physics of dynamic Hubbard models as opposed to conventional Hubbard models: when a second electron (of opposite spin) is added to a non-degenerate orbital, it expands. We can describe this physics by a multi-orbital tight binding model (at least two orbitals per site)[9, 82], or with a background spin[4, 10] or harmonic oscillator[83, 84] degree of freedom that is coupled to the electronic double occupancy, as in Eq. (2). Assuming the latter, the site Hamiltonian is given by Eq. (3), and the Hamiltonian can be written as

$$H = - \sum_{i,j,\sigma} [t_{ij} c_{i\sigma}^\dagger c_{j\sigma} + h.c.] + \sum_i \hbar\omega_0 a_i^\dagger a_i + \sum_i [U + g\hbar\omega_0](a_i^\dagger + a_i)n_{i\uparrow}n_{i\downarrow} \quad (4)$$

with frequency $\omega_0 = \sqrt{K/m}$ and $g = \alpha/(2K\hbar\omega_0)^{1/2}$ the dimensionless coupling constant. Estimates for the values of these parameters were discussed in ref. [11]. In particular, for $1s$ orbitals $g^2\omega_0 \sim 4.1\text{eV}$. Quite generally we expect g to increase proportionally to $1/Z$ and ω_0 to

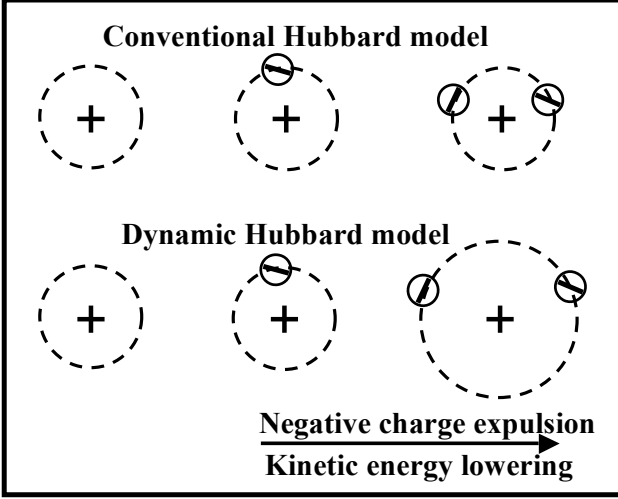


FIG. 1: In the conventional Hubbard model the atomic orbital is not modified by electronic occupancy. In the dynamic Hubbard model and in real atoms, addition of the second electron causes orbital expansion due to the electron-electron interaction. Negative charge is expelled outward and the kinetic energy of the electrons is lowered relative to that with a non-expanded orbital.

increase proportionally to Z^2 , where Z is the charge of the ion when the orbital under consideration is empty[11]. However, in an even more realistic model ω_0 should also change with different electronic occupation. That issue is beyond the scope of this paper.

Using a generalized Lang-Firsov transformation[11, 85–87] the electron creation operator $c_{i\sigma}^\dagger$ is written in terms of new quasiparticle operators $\tilde{c}_{i\sigma}^\dagger$ as

$$c_{i\sigma}^\dagger = e^{g(a_i^\dagger - a_i)\tilde{n}_{i,-\sigma}} \tilde{c}_{i\sigma}^\dagger = [1 + (e^{-g^2/2} - 1)\tilde{n}_{i,-\sigma}] \tilde{c}_{i\sigma}^\dagger + \tilde{n}_{i,-\sigma} \times (\text{incoherent part}) \quad (5)$$

where the incoherent part describes the processes where the boson goes into an excited state when the electron is created at the site. For large ω_0 those terms become small and can be neglected, and even for not so large ω_0 we have found from numerical studies that their effect does not change the low energy physics qualitatively[88, 89]. Hence we will ignore those terms in what follows, which amounts to keeping only ground state to ground state transitions of the boson field.

The electron creation operator is then given by

$$c_{i\sigma}^\dagger = [1 + (S - 1)\tilde{n}_{i,-\sigma}] \tilde{c}_{i\sigma}^\dagger \quad (6a)$$

$$S = e^{-g^2/2} \quad (6b)$$

and the quasiparticle weight for electronic band filling n (n electrons per site) is

$$z(n) = (1 + (S - 1)\frac{n}{2})^2 \quad (6c)$$

so that it decreases monotonically from 1 when the band is almost empty to $S^2 < 1$ when the band is almost full. The single particle Green's function and associated spectral function is renormalized by the multiplicative factors on the quasiparticle operators given in Eq. (6a)[86], which on the average amounts to multiplication of the spectral function by the quasiparticle weight Eq. (6c). This will cause a reduction in the photoemission spectral weight at low energies from what would naively follow from the low energy effective Hamiltonian, an effect extensively discussed in Ref. [86] and recently rediscovered in [20]. A corresponding reduction occurs in the two-particle Green's function and associated low frequency optical properties[86, 88].

The low energy effective Hamiltonian is then

$$H = - \sum_{ij\sigma} t_{ij}^\sigma [\tilde{c}_{i\sigma}^\dagger \tilde{c}_{j\sigma} + h.c.] + U_{eff} \sum_i \tilde{n}_{i\uparrow} \tilde{n}_{i\downarrow} \quad (7a)$$

$$t_{ij}^\sigma = [1 + (S - 1)\tilde{n}_{i,-\sigma}][1 + (S - 1)\tilde{n}_{j,-\sigma}] t_{ij} \quad (7b)$$

and $U_{eff} = U - \hbar\omega_0 g^2$. Thus, the hopping amplitude for an electron between sites i and j is given by t_{ij} , St_{ij} and $S^2 t_{ij}$ depending on whether there are 0, 1 or 2 other electrons of opposite spin at the two sites involved in the hopping process.

The physics of these models is determined by the magnitude of the parameter S , which can be understood as the overlap matrix element between the expanded and unexpanded orbital in Fig. 1. It depends crucially on the net ionic charge Z , defined as the ionic charge when the orbital in question is unoccupied[11]. In Fig. 1, $Z = 1$ if the states depicted correspond to the hydrogen ions H^+ , H and H^- and $Z = 2$ if they correspond to He^{++} , He^+ and He . In a lattice of $O^{=}$ anions, as in the $Cu - O$ planes of high T_c cuprates, the states under consideration are O , O^- and $O^{=}$ and $Z = 0$, and in the B^- planes of MgB_2 , $Z = 1$. The effects under consideration here become larger when S is small, hence when Z is small. An approximate calculation of S as function of Z is given in [11].

We now perform a particle-hole transformation since we will be interested in the regime of low hole concentration. The hole creation operator is given by, instead of Eq. (6a)

$$c_{i\sigma}^\dagger = [S + (1 - S)\tilde{n}_{i,-\sigma}] \tilde{c}_{i\sigma}^\dagger \quad (8a)$$

where $\tilde{n}_{i,\sigma}$ is now the hole site occupation, and the hole quasiparticle weight increases with hole occupation n as

$$z_h(n) = S^2 (1 + (\frac{1}{S} - 1)\frac{n}{2})^2 \quad (8b)$$

For simplicity of notation we denote the hole creation operators again by $c_{i\sigma}^\dagger$, the hole site occupation by $n_{i\sigma}$ and the effective on-site repulsion between holes of opposite spin U_{eff} (the same as between electrons) by U to

simplify the notation. The Hamiltonian for holes is then

$$H = - \sum_{ij\sigma} t_{ij}^\sigma [c_{i\sigma}^\dagger c_{j\sigma} + h.c.] + U \sum_i n_{i\uparrow} n_{i\downarrow} \quad (9a)$$

$$t_{ij}^\sigma = t_{ij}^h [1 + (\frac{1}{S} - 1)n_{i,-\sigma}] [1 + (\frac{1}{S} - 1)n_{j,-\sigma}] t_{ij} \quad (9b)$$

with $t_{ij}^h = S^2 t_{ij}$ the hopping amplitude for a single hole when there are no other holes in the two sites involved in the hopping process. The hole hopping amplitude and the effective bandwidth increase as the hole occupation increases, and so does the quasiparticle (quasihole) weight Eq. (8b).

Finally, we will assume there is only nearest neighbor hopping $t_{ij} = t$ for simplicity and write the nearest neighbor hopping amplitude resulting from Eq. (9b) as

$$t_{ij}^\sigma = t_h + \Delta t (n_{i,-\sigma} + n_{j,-\sigma}) + \Delta t_2 n_{i,-\sigma} n_{j,-\sigma} \quad (10a)$$

with

$$t_h = tS^2 \quad (10b)$$

$$\Delta t = tS(1 - S) \quad (10c)$$

$$\Delta t_2 = t(1 - S)^2 = (\Delta t)^2 / t_h. \quad (10d)$$

The non-linear term with coefficient Δt_2 is expected to have a small effect when the band is close to full (with electrons) and is often neglected. Without that term, the model is also called generalized Hubbard model or Hubbard model with correlated hopping[90, 91]. The effective hopping amplitude for average site occupation n is, from Eq. (10a)

$$t(n) = t_h + n\Delta t + \frac{n^2}{4}\Delta t_2 \quad (11)$$

so that a key consequence of integrating out the higher energy degrees of freedom is to renormalize the hopping amplitude and hence the bandwidth and the effective mass (inverse of hopping amplitude), as emphasized since the beginning of our studies of these Hamiltonians [92] and recently rediscovered in a different context[20].

III. GENERALIZED DYNAMIC HUBBARD MODELS

More generally, one can assume that the boson degree of freedom will couple not only to the double orbital occupancy but also to the singly occupied orbital[86]. The site Hamiltonian is then

$$H_i = \hbar\omega_0 a_i^\dagger a_i + \hbar\omega_0 [gn_{i\uparrow}n_{i\downarrow} + g_0(n_{i\uparrow} + n_{i\downarrow})] \quad (12)$$

At the atomic level, the coupling g_0 will appear when considering an orbital for atoms other than hydrogenic ones, and represents the modification of the states of electrons in other orbitals in the atom when the first electron is created in the orbital under consideration. We expect this effect to be much smaller than the modification of the state of the electron residing in the same orbital, the physics described by g , hence $g_0 \ll g$, particularly when the ionic charge Z is small. The formal development for the site Hamiltonian given by Eq. (12) is very similar to the one discussed in the previous section and is given in Ref. [86]. In particular, Eq. (6) becomes

$$c_{i\sigma}^\dagger = [T + (S - T)\tilde{n}_{i,-\sigma}]\tilde{c}_{i\sigma}^\dagger \quad (13a)$$

$$T = e^{-g_0^2/2} \quad (13b)$$

$$S = e^{-(g+g_0)^2/2} \quad (13c)$$

$$z(n) = (T + (S - T)\frac{n}{2})^2. \quad (13d)$$

and of course $S < T$ always [10] since $g > 0$. The hopping amplitudes given in the previous section are similarly modified by replacing 1 by T in various places, as discussed in Ref. [86]. g_0 gives a renormalization of the quasiparticle mass, bandwidth and quasiparticle weight that is independent of band filling, and g gives a band-filling dependent contribution.

Recently, a single band model with site Hamiltonian of the form Eq. (12) with $g = 0$ and $g_0 \neq 0$ was considered[20] to describe the effect of higher energy electronic excitations on the low energy electronic physics within dynamical mean field theory[93]. In our view this is an unphysical limit since we expect $g \gg g_0$ quite generally. Some of the effects discussed in refs. [11, 86, 88, 89, 92] were rediscovered in that work[20], in particular the “bandwidth renormalization from Coulombic screening”, the “renormalization of the hopping and hybridization parameters”, and the fact that “the photoemission spectral weight in the frequency range described by the effective model is reduced”, as well as the fact that the effective model “gives a reasonable good description” even if w_0 is not too large[20]. The effects specifically associated with $g \neq 0$ will presumably be rediscovered when the authors of Ref. [20] include g in their Hamiltonian, as well as the effect on two-particle Green’s functions and optical properties discussed in [10], [21], [57], [82] and [88], when the authors of Ref. [20] consider those quantities.

IV. HOLE PAIRING AND SUPERCONDUCTIVITY IN DYNAMIC HUBBARD MODELS

As we[55] and others[94–97] have discussed, the correlated hopping Δt gives a strong tendency to pairing and

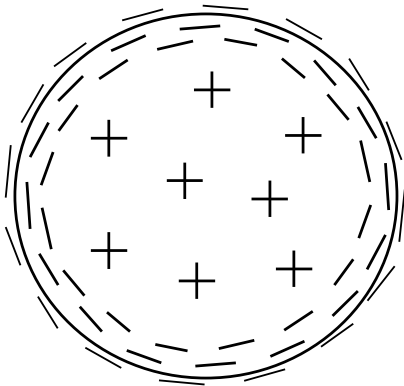


FIG. 2: Expected charge distribution in the ground state of superconductors according to the theory of hole superconductivity[25].

superconductivity when a band is almost full. The hopping amplitude for a single hole is t_h , and it increases to $t_h + \Delta t$ when the hole hops to or from a site occupied by another hole (of opposite spin), thus giving an incentive for holes to pair to lower their kinetic energy. The superconductivity described by this model has a number of interesting features[55] that we have proposed are relevant to the description of high T_c cuprates, namely strong dependence of T_c on hole concentration[55], energy dependent gap function and resulting tunneling asymmetry of universal sign[98], superconductivity driven by kinetic energy lowering and associated low energy optical sum rule violation[56], change in optical spectral weight at frequencies much higher than the superconducting energy gap upon onset of superconductivity[10], strong positive pressure dependence of T_c [55], increased quasiparticle weight upon entering the superconducting state[86], etc. Many of these predictions are supported by observations on high T_c cuprates made both before and after the predictions were made.

The more fundamental dynamic Hubbard model from which the Δt interaction derives has also been studied using Eliashberg theory[89] and exact numerical methods[88] and shows an even stronger tendency to pairing and superconductivity.

V. NEGATIVE CHARGE EXPULSION IN DYNAMIC HUBBARD MODELS

Within the theory of hole superconductivity, superconductors are predicted to have a non-homogeneous charge distribution in the ground state[24], as shown schematically in Fig. 2: excess positive charge in the interior and excess negative charge near the surface, resembling a “giant atom”[99]. This charge distribution is predicted from modified London-like electrodynamic equations[25]. As we will see here, dynamic Hubbard models predict qualitatively similar behavior.

We consider the Hamiltonian for holes Eq. (9), with the hopping amplitudes given by Eq. (10), which we reproduce here for convenience:

$$H = - \sum_{ij\sigma} t_{ij}^{\sigma} [c_{i\sigma}^{\dagger} c_{j\sigma} + h.c.] + U \sum_i n_{i\uparrow} n_{i\downarrow} \quad (14a)$$

$$t_{ij}^{\sigma} = t_h + \Delta t(n_{i,-\sigma} + n_{j,-\sigma}) + \Delta t_2 n_{i,-\sigma} n_{j,-\sigma} \quad (14b)$$

It is clear from the form of this Hamiltonian that the kinetic energy decreases when the number of holes in the band increases, since the hopping amplitudes Eq. (14b) increase with hole occupation. This suggests that the system will have a tendency to *expel electrons* from its interior to the surface, because the coordination of sites in the interior is larger than of sites at the surface. In what follows we study this physics numerically.

We assume a cylindrical geometry of radius R and infinite length in the z direction. We decouple the interaction terms within a simple mean field approximation assuming $\langle n_{i\sigma} \rangle = n_i/2$ with n_i the hole occupation at site i , and obtain the mean field Hamiltonian

$$H_{mf} = H_{mf,kin} + H_{mf,pot} \quad (15a)$$

$$H_{mf,kin} = - \sum_{\langle ij \rangle, \sigma} [t_h + \Delta t n_i + \Delta t_2 \frac{n_i^2}{4}] [c_{i\sigma}^{\dagger} c_{j\sigma} + h.c.] \quad (15b)$$

$$H_{mf,pot} = \frac{U}{4} \sum_i n_i^2 \quad (15c)$$

Assuming a band filling of n holes per site, we diagonalize the Hamiltonian Eq. (15) with initial values $n_i = n$ and fill the lowest energy levels until the occupation n is achieved. From the Slater determinant of that state we obtain new values of n_i for each site, and iterate this procedure until self-consistently is achieved. We can extend this procedure to finite temperatures, iterating to self-consistency for a given chemical potential μ . We consider then the resulting occupation of the sites as function of the distance r to the center of the cylinder. Sometimes there are non-equivalent sites at the same distance from the origin (e.g. (5,0) and (3,4)) that yield somewhat different occupation, for those cases we show the average and standard deviation as error bars in the graphs.

Figure 3 shows a typical example of the behavior found. Here we assumed $\Delta t_2 = 0$, corresponding to the simpler Hubbard model with correlated hopping and no six-fermion operator term. Even for $\Delta t = 0$ the hole occupation is somewhat larger in the interior than near the surface. When the interaction Δt is turned on, the hole occupation increases in the interior and decreases near the surface. This indicates that the system expels electrons from the interior to the surface. The effect becomes more pronounced when Δt is increased.

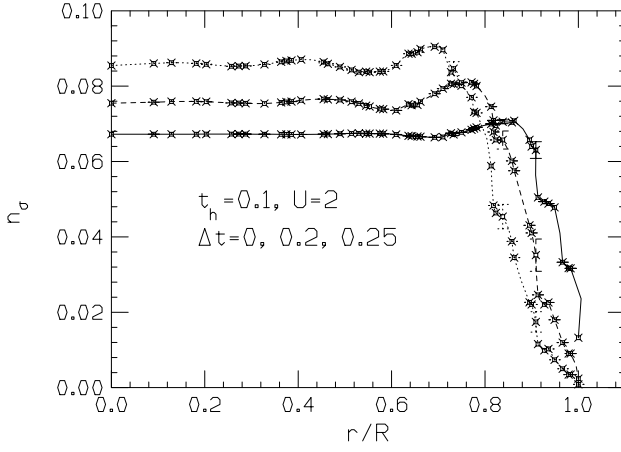


FIG. 3: Hole site occupation per spin for a cylinder of radius $R = 11$ as function of r/R , with r the distance to the center, for a cubic lattice of side length 1. There are 377 sites in a cross-sectional area ($\pi R^2 = 380.1$). The average occupation (both spins) is $n = 0.126$ holes per site and the temperature is $k_B T = 0.02$.

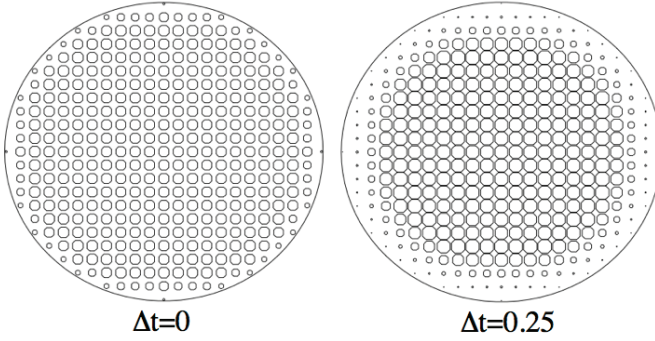


FIG. 4: The diameters of the circles are proportional to the hole occupation of the site. Note that for finite Δt the hole occupation increases in the interior and is depleted near the surface. The parameters correspond to the cases shown in Fig. 3.

Figure 4 shows the hole site occupations as circles of diameter proportional to it, for the cases $\Delta t = 0$ and $\Delta t = 0.25$ of Fig. 3. Note that the interior hole occupation is larger for $\Delta t = 0.25$ than it is for $\Delta t = 0$, while near the surface the hole occupation is larger for $\Delta t = 0$. Again this shows that the system with $\Delta t = 0.25$ is expelling electrons from the interior to the surface, thus depleting the hole occupation near the surface.

These results are obtained by iteration. Fig. 5 shows the behavior of the energies as a function of iteration number for the cases $\Delta t = 0$ and $\Delta t = 0.25$ of Fig. 3. The initial values correspond to a uniform hole distribution with each site having the average occupation. The evolution is non-monotonic because in the intermediate steps the overall hole concentration increases, nevertheless it can be seen that for the case $\Delta t = 0.25$ the final kinetic energy when self-consistency is achieved is

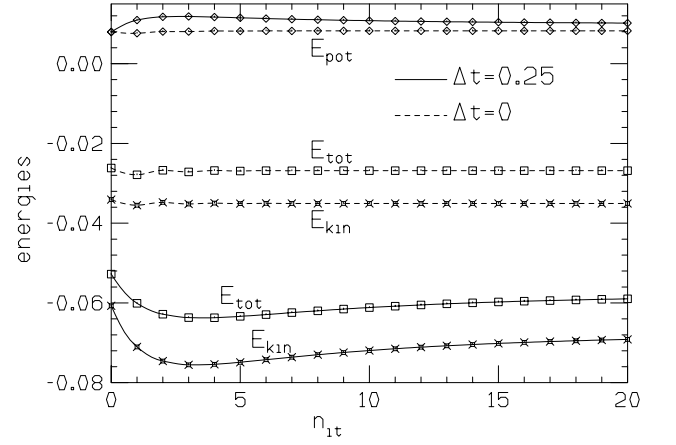


FIG. 5: Kinetic, potential and total energy per site for $\Delta t = 0.25$ as function of number of iterations starting with a uniform hole distribution.

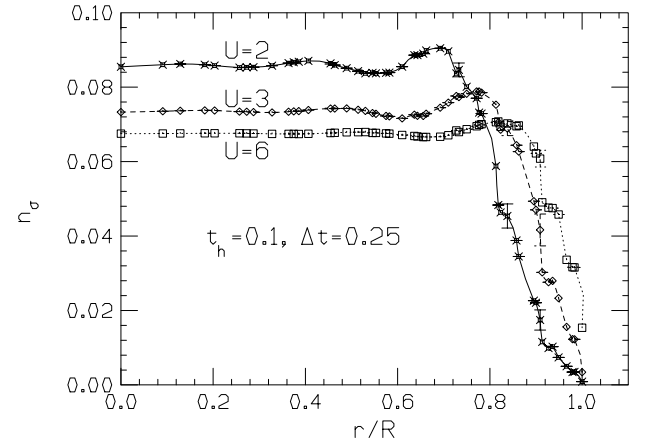


FIG. 6: Effect of Coulomb repulsion. $t_h = 0.1$, $\Delta t = 0.25$. As the on-site repulsion increases, the charge expulsion decreases and the occupation becomes more uniform.

lower, and the final potential energy is higher, associated with the larger hole concentration in the interior and the lower hole concentration near the surface shown in Fig. 4. This is of course what is expected. For the case $\Delta t = 0$ instead there is essentially no difference in the energies between the initial uniform state and the final self-consistent state.

The charge expulsion caused by Δt is counteracted by the effect of Coulomb repulsion, just like the tendency to pairing is [55]. Figure 6 shows the effect of increasing the on-site repulsion for a fixed value of Δt .

The effect of the non-linear occupation-dependent hopping term Δt_2 (Eq. (10d)) is shown in Fig. 7. It increases the charge expulsion tendency relative to the model where this term is omitted (Hubbard model with correlated hopping).

As the correlated hopping amplitude Δt increases, and even more so in the presence of Δt_2 , the system appears

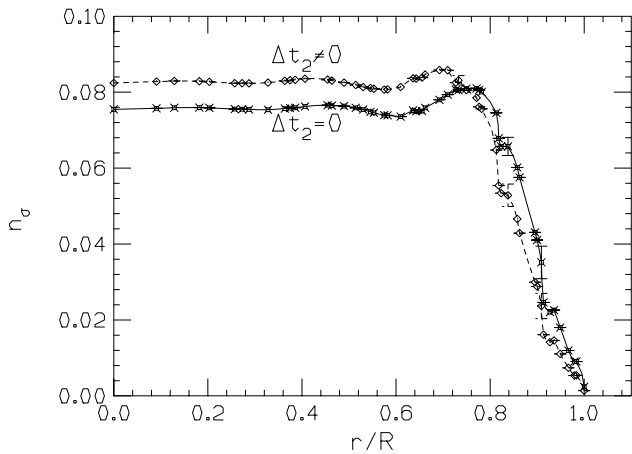


FIG. 7: Effect of non-linear occupation-dependent hopping term Δt_2 , Eq. (7c) for the case $\Delta t = 0.25$ of Fig. 3.

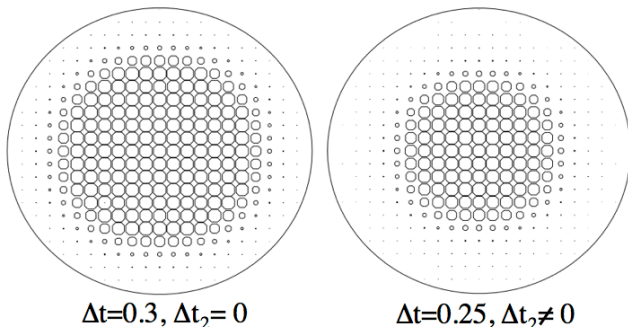


FIG. 8: As the correlated hopping terms increase, the system develops a tendency to phase separation, where essentially all the holes condense to the interior. Parameters are the same as in Fig. 3 except as indicated. The maximum hole occupation per spin is 0.128 and 0.214 for the left and right panel, the average hole occupation per spin is 0.063.

to develop a tendency to phase separation, where holes condense in the interior and the outer region of the cylinder becomes essentially empty of holes. This happens very rapidly as function of the parameters for the finite system under consideration. Examples are shown in Fig. 8. We return to this point in the next section.

The charge expulsion tendency and associated effects described in this and other sections become rapidly weaker when the hole concentration increases. To illustrate this we show in Fig. 9 the charge distribution for the same Hamiltonian parameters as Fig. 8 but average hole occupation per site $n = 0.35$ instead of $n = 0.126$. It can be seen that the charge expulsion is much smaller.

In summary, we have seen in this section that the dynamic Hubbard model promotes expulsion of negative charge from the interior to the surface of the system when the band is almost full, and that the charge expulsion physics is associated with kinetic energy lowering, just as in the single atom, Fig. 1. The charge expulsion tendency is largest when the parameter Δt is largest, which in turn

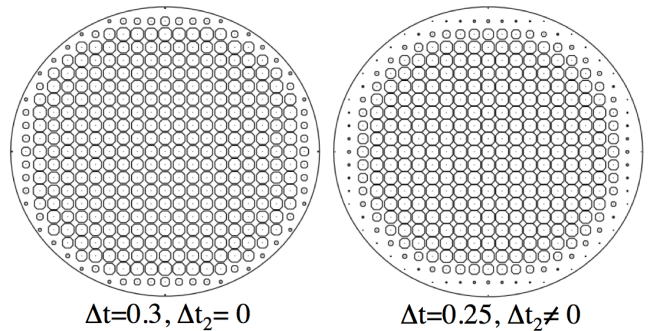


FIG. 9: Hole site occupations for the same parameters as Fig. 8 but average hole occupation per spin 0.175. The maximum hole occupation per spin is 0.107 for the left panel, 0.116 for the right panel.

corresponds to smaller S , the overlap of the atomic orbitals when one and two electrons are at the orbital. As discussed earlier, S is smaller when the ionic charge Z is smaller, corresponding to a more negatively charged ion. The fact that the effective Hamiltonian derived from this physics expels more negative charge the more negatively charged the ion is makes of course a lot of sense and can be regarded as an internal consistency check on the validity of the model.

For a normal metal, the charge expulsion physics will be compensated to a large extent by other effects since no electric field can exist in the interior of a normal metal. The Coulomb repulsion will do this, but as we argue in the next sections some residual effects of charge expulsion can be seen even in the normal state. For the superconducting state, we have proposed new electrodynamic equations that give rise to “charge rigidity” [100] and the inability of the superfluid to screen interior electric fields so that the charge expulsion physics can manifest itself [25].

VI. PHASE SEPARATION

The tendency to charge expulsion in the dynamic Hubbard model can also lead to a thermodynamic instability and ensuing phase separation. The question of phase separation in these models in certain parameter ranges was recently considered by Montorsi and coworkers [101, 102].

Let us consider the correlated hopping model first for simplicity ($\Delta t_2 = 0$). The effective hopping amplitude for a hole is $t(n) = t_h + n\Delta t$ with n the hole density per site. In the dilute limit, the kinetic energy of a hole is $\epsilon = -zt(n)$, with z the number of nearest neighbors to a site, and it is clear that when Δt is much larger than t_h putting for example all holes into half the system and thus emptying the other half will double n and hence decrease the kinetic energy per hole as well as the total energy if it is dominated by kinetic energy. This tendency to phase separation will be countered both by Pauli exclusion and by Coulomb repulsion.

Consider a flat density of states for simplicity. The effective bandwidth increases linearly with n

$$D(n) = D_h + Kn \quad (16)$$

with $D = 2zt$, $D_h = 2zt_h$, $K = 2z\Delta t$. The density of states per site per spin is given by $g(\epsilon) = 1/D$ and the ground state kinetic energy by

$$E_{kin} = \int_{-D/2}^{\mu} \epsilon g(\epsilon) d\epsilon = \frac{D}{4}(n^2 - 2n) \quad (17)$$

with $\mu = (n - 1)D(n)/2$ the chemical potential for n holes per site. Adding the on-site repulsion in a mean field approximation yields

$$E_o(n) = \frac{D_h + nK}{4}(n^2 - 2n) + \frac{U}{4}n^2 \quad (18)$$

and the system will be unstable towards phase separation into hole-rich and hole-poor regions when the condition

$$\frac{\partial^2 E_o}{\partial n^2} = \frac{U + D_h}{2} + K(\frac{3}{2}n - 1) < 0 \quad (19)$$

is satisfied, hence

$$K > \frac{U + D_h}{2(1 - \frac{3}{2}n)} \quad (20)$$

or equivalently

$$\Delta t > \frac{t_h + U/(2z)}{2(1 - \frac{3}{2}n)}. \quad (21)$$

For the parameters used in the previous section, e.g. $t_h = 0.1$, $n = 0.126$, $U = 2$ and $z = 4$ appropriate to two dimensions Eq. (21) yields $\Delta t > 0.216$. The tendency to phase separation becomes even stronger when the nonlinear term Δt_2 is included. After some simple algebra Eq. (21) is modified to the condition

$$\Delta t > \frac{t_h + U/(2z)}{2(1 - \frac{3}{2}n)} - \frac{3\Delta t^2 n(1 - n)/(4t_h)}{2(1 - \frac{3}{2}n)} \quad (22)$$

which for the parameters given above yields $\Delta t > 0.182$. These estimates are consistent with the numerical results shown in the previous section. Note that as n increases larger Δt is needed for phase separation.

Note that the instability criterion Eq. (19) appears to be different from the usual criterion

$$\frac{\partial \mu}{\partial n} < 0 \quad (23)$$

if μ is given by the expression given right after Eq. (17). The reason is that the μ in Eq. (17) is not the true chemical potential but an effective one. The true chemical potential is modified by contributions from both the Hubbard repulsion and the density dependent hopping terms. For the case with $\Delta t_2 = 0$ it is given by

$$\mu = \mu_{eff} + \frac{Un}{2} - \frac{K}{2} < c_{i\sigma}^\dagger c_{j\sigma} + h.c. > \quad (24a)$$

$$\mu_{eff} = \frac{D_h + nK}{2}(n - 1) \quad (24b)$$

$$< c_{i\sigma}^\dagger c_{j\sigma} + h.c. > = n(1 - \frac{n}{2}) \quad (24c)$$

where the expectation value for the bond charge Eq. (24c) follows from Eq. (17). Hence we obtain from Eq. (24)

$$\frac{\partial \mu}{\partial n} = \frac{U + D_h}{2} - K(1 - \frac{3}{2}n) \quad (25)$$

in agreement with Eq. (19). The instability criteria Eq. (23) or Eq. (19) with the free energy replacing E_o , are also valid at finite temperature of course.

In a real material in the normal state phase separation will not occur because of the effect of longer-range Coulomb interactions. However this physics will clearly favor charge inhomogeneity, i.e. hole-rich regions that benefit from the lowering of kinetic energy acquired by increasing the hole concentration and thereby broadening the (local) bandwidth, and hole-poor regions where the kinetic energy cost is mitigated by narrowing of the local bandwidth. The shape of these regions will depend on the particular details of the system and merits further investigation. A possible geometry for the hole-rich and hole-poor regions could be one-dimensional, i.e. stripes[62]. Other geometries like patches are also possible[64, 65]. Such charge inhomogeneities are commonly seen in high T_c superconductors[61] where the physics discussed here should be dominant.

VII. CHARGE INHOMOGENEITY

High T_c cuprates show a high tendency to charge inhomogeneity[61, 63–65]. We suggest that a dynamic Hubbard model may be relevant to describe this physics: because kinetic energy dominates the physics of the dynamic Hubbard model, the system will develop charge inhomogeneity at a cost in potential energy if it can thereby lower its kinetic energy more, unlike models where the dominant physics is potential (correlation) energy like the conventional Hubbard model.

Let us consider the effect of local potential variations. We have shown before that in the superconducting state of the model with Δt there is great sensitivity to local potential variations due to the slope of the gap function[103]. Here we find that the model is also sensitive to local potential variations in the normal state.

We assume there are impurities in the system that change the local potential at some sites, and compare the effect of such perturbations for the dynamic and conventional Hubbard models. As an example we take parameters $t_h = 0.1$, $U = 2$ and consider site impurity potentials of magnitude ± 0.2 at several sites as indicated in the caption of Fig. 9. For the dynamic Hubbard model we take $\Delta t = 0.2$, $\Delta t_2 = 0.4$, corresponding to $S = 0.333$.

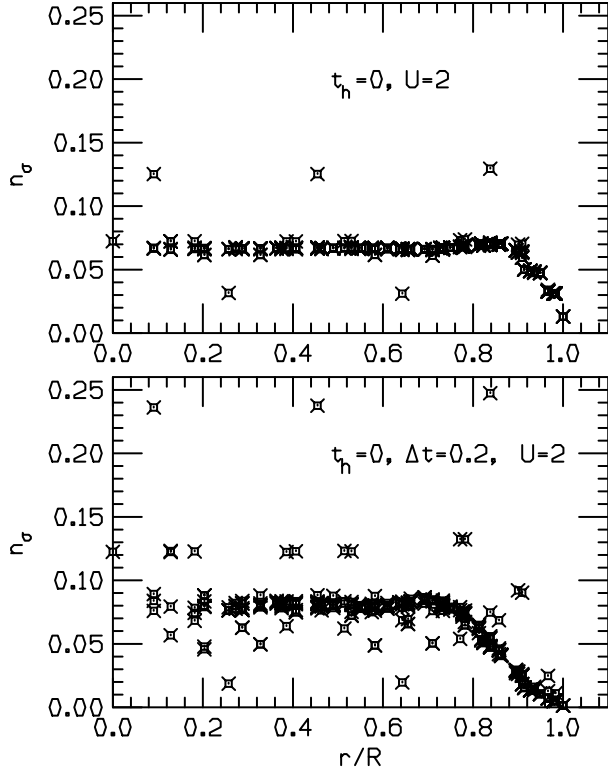


FIG. 10: Hole site occupation per spin in a system of radius $R = 11$ with 5 impurities at positions $(-1,0)$, $(2,2)$, $(3,-4)$, $(-5,-5)$, $(-6,7)$ with potential strength -0.2 , $+0.2$, -0.2 , $+0.2$, -0.2 respectively. Note the much larger variation in densities generated in the dynamic Hubbard model (lower panel, $\Delta t_2 \neq 0$) than in the conventional Hubbard model (upper panel). Average hole occupation per site is $n = 0.126$.

Figure 10 shows the effect of these impurities on the charge occupation for the conventional and dynamic models. In the conventional Hubbard model the occupation changes at the site of the impurity potential and only very slightly at neighboring sites. In the dynamic Hubbard model the local occupation change at the impurity site itself is much larger than in the conventional model, and in addition, the occupations change at many other sites in the vicinity of the impurities, as seen in the lower panel of Figure 10. Figure 11 shows the real space distribution of these changes.

Similarly we can consider impurities where the atomic value of the deformation parameter S is different than in the bulk. This would occur for example by substituting an ion by another ion with different ionic charge, hence different orbital rigidity. For example, substituting O^{--} by F^- would make the orbital more rigid and increase S at this site, while substituting O^{--} by N^{---} would make the orbital more floppy and decrease S . Figure 12 shows 5 impurities at the same locations as in Figure 9, with values $S = 0.5$ and 0.2 at the impurity sites instead of the bulk value $S = 1/3$. The larger (smaller) S will increase (decrease) the occupation. Compared to the case

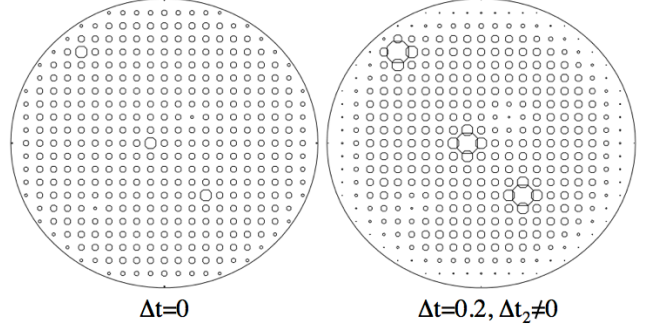


FIG. 11: The site occupations for the case of Fig. 10, with the diameters of the circles proportional to the hole occupation of the sites. Note the 5 impurity sites at positions listed in the caption of Fig. 9 (three with negative potential, hence higher hole concentration) and two with positive potential, hence lower hole concentration. Note that for $\Delta t = 0$ only the occupation at the impurity site changes appreciably, while for $\Delta t \neq 0$ an impurity potential of the same strength causes a much larger change of the occupation at the impurity site and occupation change also at the nearest and next nearest neighbor sites.

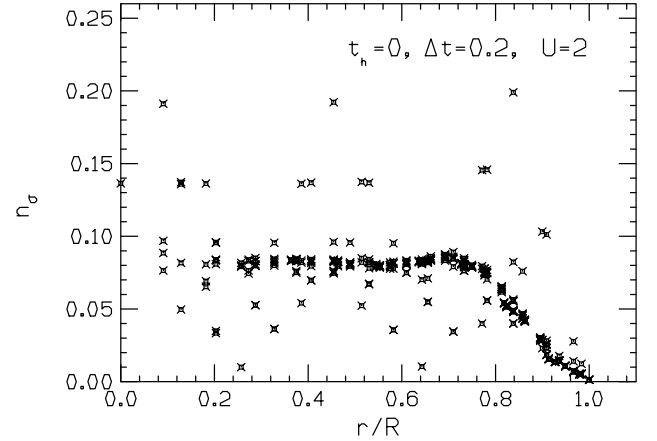


FIG. 12: Hole site occupation per spin in a system of radius $R = 11$ with 5 impurities at positions $(-1,0)$, $(2,2)$, $(3,-4)$, $(-5,-5)$, $(-6,7)$ with S factor 0.5 , 0.2 , 0.5 , 0.2 , 0.5 respectively. All other sites have $S = 0.333$. $n = 0.126$. Note that the variations in density occur for even more sites than when the local potential is changed, Fig. 10 lower panel, even though the change in occupation at the impurity site itself is smaller.

of Fig. 10, it can be seen that the change in occupation at the impurity site itself is somewhat smaller for these parameters but the changes are larger at neighboring sites and extend to sites farther away. Similarly as in Fig. 11 we show the real space changes in Figure 13, compared to the conventional Hubbard model where no change at all would occur since it is not sensitive to the rigidity of the orbital.

The changes in site energies in the example of Figs. 10 and 11 could occur both if there are substitutional impurities in the conducting plane with different on-site ener-

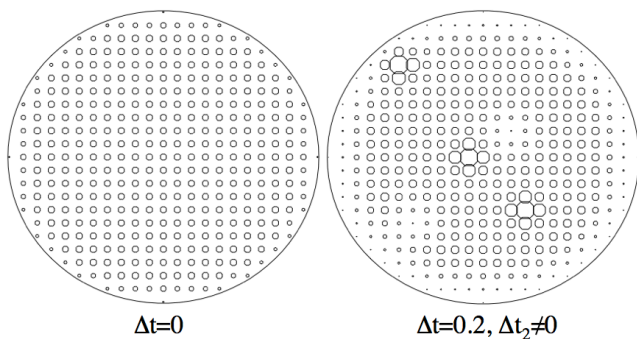


FIG. 13: The site occupations for the case of Fig. 11, with the diameters of the circles proportional to the hole occupation of the sites. Same 5 impurity sites at positions listed in the caption of Fig. 10 (three with larger S , hence higher hole concentration) and two with smaller S , hence lower hole concentration. Note that the range of sites where the occupation changes is even larger than in Fig. 11, extending to third nearest neighbors. The left panel shows for comparison a uniform system, corresponding to a conventional Hubbard model that does not take into account the deformation of the orbital, hence $S = 1$ for all sites.

gies, or if there are impurities off the plane that change the local potential in the plane. In contrast, the example of Figs. 12 and 13 would be appropriate to describe only impurities in the plane itself where the electrons conduct.

The reason for this large sensitivity to local perturbations can be understood from the form of the hopping amplitude Eq. (14b). A change in the local occupation will also change the hopping amplitude of a hole between that site and neighboring sites, which in turn will change the occupation of neighboring sites, and so on. Similarly a change in the deformation parameter S at a site will affect the hopping amplitudes between that site and its nearest neighbors, hence the occupation of the site and its neighbors, etc. In that way a local perturbation in the dynamic Hubbard model gets amplified and expanded to its neighboring region, and it is easy to understand how a non-perfect crystal will easily develop patches of charge inhomogeneity in the presence of small perturbations. These inhomogeneities cost potential (electrostatic) energy, but are advantageous in kinetic energy. The conventional Hubbard model does not exhibit this physics.

VIII. GRAIN BOUNDARIES IN HIGH T_c CUPRATES

The high superconducting transition temperature of the cuprates indicate that, if they are described by dynamic Hubbard models, they have a small value of the parameter S or equivalently a large value of the correlated hopping parameter Δt . This is to be expected because of the small ionic charge associated with the negative ion O^\ominus . According to the results of the previous

sections, this should lead to a strong tendency of high T_c cuprates to expel negative charge from their interior and to develop charge inhomogeneity in the presence of disorder. In this section we argue that these features may also be relevant to the understanding of properties of grain boundaries in high T_c cuprates[104–106].

Babcock et al[107] report results of EELS experiments indicating severe hole depletion in YBCO near grain boundaries for large angle grain boundaries, with the hole deficient region extending up to 100\AA or more into the crystal. In contrast, small angle grain boundaries show significantly less hole depletion. It is reasonable to assume that for larger angle grain boundaries there is weaker coupling between the grains, and this is confirmed experimentally by measurement of the Josephson critical current across the grain boundary[107]. Furthermore, Babcock et al found that the structural changes associated with the grain boundaries (structural perturbations and cation nonstoichiometry) extended only about 5\AA from the grain boundary into the crystal, and that the hole depletion is not associated with particular specimen preparation procedures such as time duration of oxygen annealing and storage conditions. The fact that the hole depletion region extends over a much wider region that associated with structural changes suggests an intrinsic purely electronic origin for the effect. Other workers have found similar results, including Browning et al[108] and Schneider et al[109].

Furthermore and consistent with this picture, it has been found that substituting Y by Ca near grain boundaries is an efficient way to prevent the hole depletion phenomenon[110–112], since Ca^{++} ions will donate fewer electrons to the CuO planes than the Y^{+++} ions they substitute, thus increasing the hole concentration and thereby improving the transport properties across the grain boundary.

Previous theoretical explanations of these effects have implicitly or explicitly assumed that grain boundaries in high T_c cuprates have an intrinsic *positive charge* that leads to band bending and consequently a flow of conduction electrons to the vicinity of the grain boundaries that causes hole depletion[113–115]. However, these explanations are directly contradicted by experiments that measure the electric potential at the grain boundary by electron-beam holography[120]. These experiments show unequivocally that the electrostatic potential at the grain boundary is *negative* with respect to the interior[117–119].

To make sense of the electron holography results, Mannhart suggested[106] that the negative potential at the grain boundary core may cause *overdoping* of the lower Hubbard band with holes, resulting in an empty band and insulating behavior. However, this explanation would appear to be inconsistent with the experiments of Babcock et al[107] discussed above, as well as with the evidence that hole doping near the grain boundaries by Ca substituting Y improves the conduction across grain boundaries. Klie et al argue that their calculations[121]

support the hole depletion scenario (hence positive potential at the grain boundary) and that this raises question about what potential is measured in the electron holography experiments. However, Koch[122] argues that “it seems to be possible to rule out that this observation is a measurement artifact inherent to the method of electron holography”.

These seemingly contradictory observations however are consistent with the physics predicted by the model under consideration here. We model the grain boundary by assuming a smaller hopping amplitude between sites at opposite sides of the grain boundary. A large angle grain boundary would presumably have a more reduced hopping amplitude compared to a small angle grain boundary. Figure 14 shows the charge distribution resulting from our model assuming a 70% reduction in the hopping amplitude across the grain boundary (denoted by a dashed line), presumably corresponding to a fairly large angle grain boundary with significant increase in the resistance. The hole density in the vicinity of the grain boundary is significantly reduced, driven by lowering of kinetic energy of the system. As a consequence, the negative charge density becomes larger near the grain boundary, and this would give rise to a *negative electric potential* at the grain boundary, consistent with the electron holography experiments, and a depleted hole concentration around the grain boundary, consistent with the EELS experiments[107].

As a function of temperature, Schneider et al[109] and Mennema et al[123] find that increasing the temperature leads to a rapid decrease of the grain boundary resistance. We suggest that this results from an increase in the hole concentration near the grain boundary as the temperature is increased. Figure 15 shows that as the temperature is increased the hole density near the grain boundary increases substantially in the dynamic Hubbard model, and as a consequence the conductivity of the region would increase. It would be interesting to measure directly the dependence of hole depletion on temperature by EELS experiments. This has not yet been done to our knowledge.

Recent measurement of properties of grain boundaries in Fe-As superconductors[124] indicate that the behavior is similar to the high T_c cuprates. This is not surprising if the physics of both classes of materials, including their superconductivity[125], is described by dynamic Hubbard models.

We expect that negative charge expulsion from the interior of superconductors should also lead to negative charging of vortex cores in the mixed state. Such effect[126] and associated antiferromagnetic order in the vortex cores[127] has been detected experimentally in $YBa_2Cu_3O_7$.

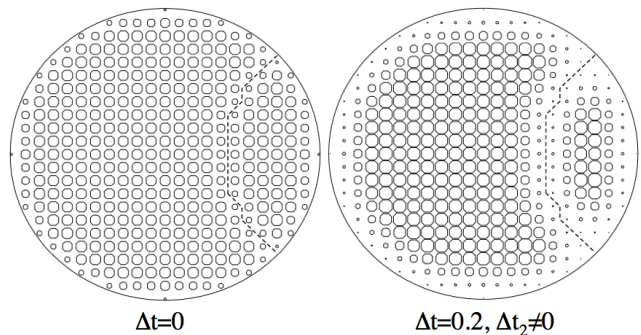


FIG. 14: Effect of a grain boundary, indicated by the dashed line for the conventional and dynamic Hubbard models with $t_h = 0.1$, $U = 2$. We assume that the hopping amplitude is reduced by a factor 0.3 for sites on opposite sides of the grain boundary. The hole occupation is depleted in the vicinity of the grain boundary in both cases, however the effect is much larger and extends over a wider range for the dynamic Hubbard model than for the conventional one. Temperature is $T = 0.02$.

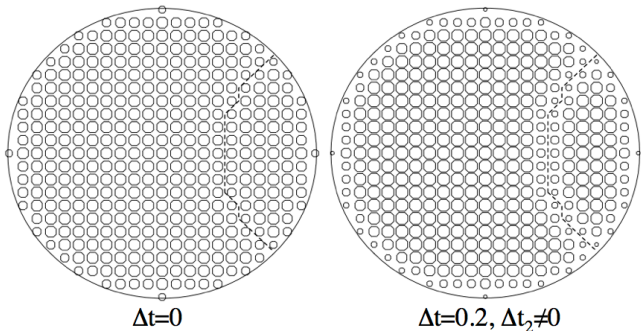


FIG. 15: Same as Fig. 14 with temperature $T = 0.1$

IX. SHAPE EFFECTS

It is interesting to consider the effect of the shape of the sample on the charge expulsion profile in the dynamic Hubbard model. Consider an ellipsoidal shape as shown in Figure 16. The sites near the surface at the regions of higher curvature, i.e. top and bottom, have somewhat smaller hole concentration than at the regions of lower curvature at the lateral surfaces. This is easy to understand: the sites near the surface in the regions of high curvature have slightly lower coordination than those in the regions of low curvature, hence the holes do not benefit so much from kinetic energy lowering and prefer to stay away from those regions. Thinking in terms of electrons instead of holes, it means the body expels more electrons to the top and bottom than to the sides. This should give rise to a higher electric potential near the sides than at the top and bottom, and a quadrupolar electric field with field lines starting at the lateral sides and ending at the top and bottom. This is precisely the type of electric field found in the superconducting state by solving the alternative London equations proposed to

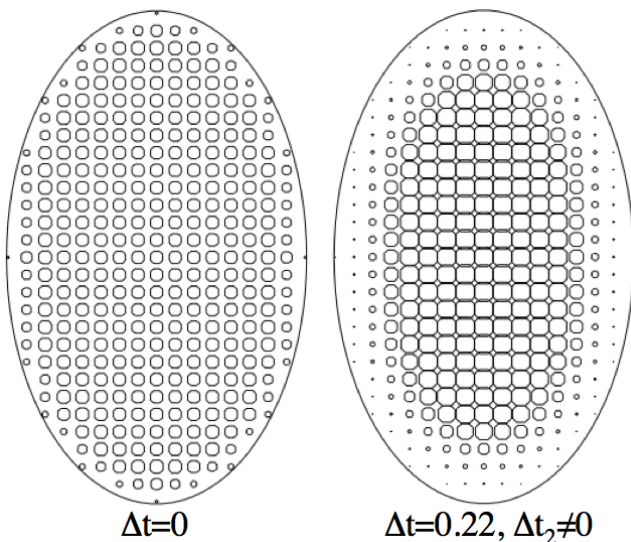


FIG. 16: Effect of shape on the charge expulsion profile. $t_h = 0.1$, $U = 2$. In the ellipsoidal shape shown, for the conventional Hubbard model the charge occupation near the surface is similar near the top surface and the lateral surfaces. For the dynamic Hubbard model the hole concentration is somewhat higher near the lateral surfaces than near the top and bottom surfaces. For the origin of this effect, see text. Temperature is $T = 0.02$.

describe the electrodynamics of superconductors within this theory[25, 128].

A qualitative way to understand this charge distribution in the superconducting state is the following: the electrons near the lateral surfaces can move faster than those at the top and bottom in the region of high curvature, just as racing cars. Hence they will have higher kinetic energy and consequently lower potential energy than the electrons near the top and bottom surfaces, so as to keep the same sum of kinetic and potential energies. Electrons near the lateral surfaces having lower potential energy means that the electric potential is higher near the lateral surfaces than near the top and bottom surfaces, resulting in electric field lines starting from the side and ending at the top and bottom just as found from the analysis of the hole distribution in the dynamic Hubbard model discussed in the above paragraph.

More generally, using the same arguments we expect that for other body shapes the electric potential will be higher in the regions of lower surface curvature and lower in the regions of higher curvature in the dynamic Hubbard model and in superconducting bodies. An example for a body shape resulting from combining a prolate and an oblate ellipsoid is given in Ref. [129].

X. CHARGE EXPULSION IN THE SUPERCONDUCTING STATE

As seen in the previous sections, the dynamic Hubbard model has a tendency to expel negative charge from its interior to the surface driven by lowering of kinetic energy. Starting with a charge neutral system in the normal state, where a uniform positive ionic charge distribution is compensated by an equal uniform negative electronic charge distribution, the negative charge expulsion would result in a net charge distribution as qualitatively shown in Fig. 2: a net excess positive charge in the interior and net excess negative charge near the surface. According to the numerical results in the previous sections (e.g. Fig. 4) the positive charge in the interior predicted by the dynamic Hubbard model Hamiltonian is approximately uniform, just as that predicted from the electrodynamic equations in the superconductor[25].

This would result in the presence of an electric field in the interior of the system, that increases linearly in going from the center towards the surface. However, this cannot happen in a real normal metal since a metal in the absence of current flow cannot have a macroscopic electric field in the interior. Therefore, we conclude that longer range Coulomb interactions, omitted in the dynamic Hubbard model, prevent this from actually taking place in a real material. In other words, potential energy triumphs over kinetic energy in the normal state, and a macroscopic metal will remain charge neutral in the interior, despite the *tendency* to develop this macroscopic charge inhomogeneity if dynamic Hubbard model physics is dominant. At most, the system will develop local charge inhomogeneity that will be screened within a Thomas Fermi length, that can be several Å in systems like underdoped high T_c cuprates where the carrier density is very low.

However, the situation can change if the system enters the superconducting state at low temperatures. There is no a-priori reason why a superconductor cannot have an electric field in its interior[25]. A superconductor is a macroscopic quantum system, and quantum systems in their ground state minimize the sum of potential and kinetic energies. That should not in general result in a uniform charge distribution that minimizes potential energy only. The electrodynamic equations that we have proposed for superconductors[25] predict that the superconductor has rigidity in the charge degrees of freedom[25, 100] and will not screen an interior electric field as a normal metal would.

To compute the charge distribution in the superconducting state we solve numerically the Bogoliubov de Gennes (BdG) equations for the dynamic Hubbard model, for systems with the same geometry as discussed in the previous sections. For the correlated hopping model ($\Delta t_2 = 0$) the equations are given in Ref. [103], and are simply extended for the case $\Delta t_2 \neq 0$. There are two gap parameters, Δ_{ii} and Δ_{ij} corresponding to on-site and nearest-neighbor pairing amplitudes[103].

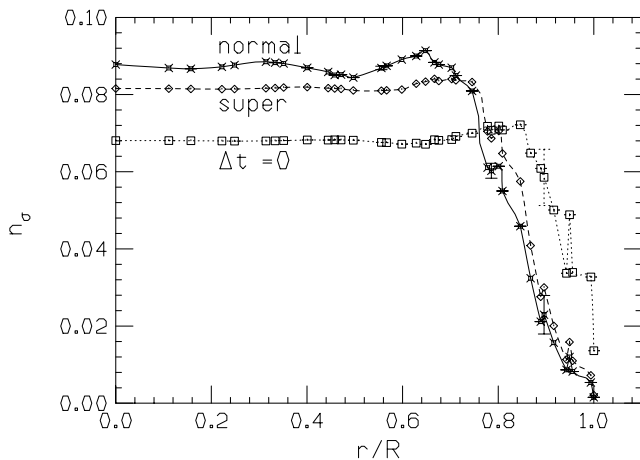


FIG. 17: Comparison of occupations in the normal and superconducting states. Radius of cylinder is $R = 9$, average occupation per site is $n = 0.126$, $t_h = 0.1$, $U = 2$, $\Delta t = 0.2$, $\Delta t_2 = 0.4$, $k_B T = 0.02$. The average gap parameters in the superconducting state are $\Delta_{ii} = 0.0044$, $\Delta_{ij} = -0.025$. We also show the occupations for the conventional Hubbard model, $\Delta t = 0 = \Delta t_2 = 0$. The charge expulsion is largest in the *normal state* of the dynamic Hubbard model.

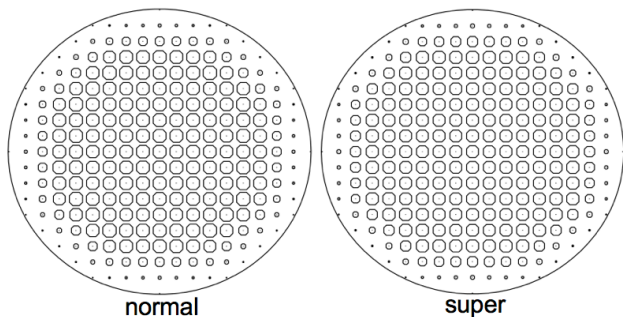


FIG. 18: Real space hole occupation for the cases of Fig. 17 with $\Delta t \neq 0$. Note that the interior hole occupation is slightly *larger* in the normal state, and the occupation near the surface slightly smaller.

We have tested our computer program by solving the BdG equations numerically on a square lattice with periodic boundary conditions and comparing with the standard BCS solution. For the cylindrical geometry with open boundary conditions considered here, the numerical solution obtained for the gap parameters deep in the interior are close to the gap parameters found in the square lattice with periodic boundary condition using both the BdG equations and the standard BCS equations applicable to translationally invariant systems. The gap parameters go to zero as the surface is approached.

Initially we had hoped[24] that comparison of the occupations in the dynamic Hubbard model in the normal and superconducting states would yield clear evidence that the system expels negative charge from the interior to the surface as it goes superconducting, as expected on

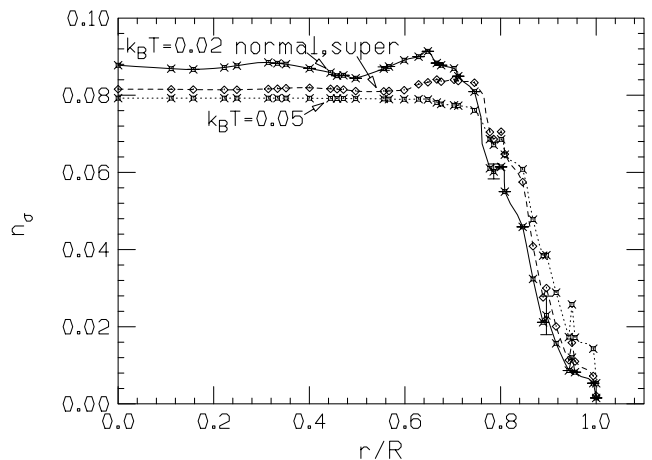


FIG. 19: Dynamic Hubbard model, parameters as in Fig. 17. Comparison of occupations right above T_c , $k_B T = 0.05$, and at $k_B T = 0.02$, with the system in the normal (full line) and superconducting (dashed line) state. Note that when the system is allowed to go superconducting, the occupations below T_c essentially don't change, while if kept in the normal state the charge expulsion increases as the temperature is lowered.

physical grounds[24, 99] and predicted by the electrodynamic equations[25]. This is *not* what happens, as shown in Figs. 17 and 18. Instead, the charge distribution becomes *more uniform* in the superconducting compared to the normal state at the same temperature. In fact, it appears that as the temperature is lowered and the system enters into the superconducting state the charge expulsion that increases in the dynamic Hubbard model as the temperature is lowered in the normal state stops changing and stays essentially the same as what it is at T_c when the system is cooled below T_c . This is shown in Figure 19.

In summary, from the numerical results presented here it appears that the BCS/BdG solution of the dynamic Hubbard model does not reflect the charge expulsion predicted by the electrodynamic equations as the system enters the superconducting state[25]. On the other hand this is perhaps not too surprising. The charge expulsion predicted by the electrodynamic equations is of the order of 1 extra electron every 10^6 sites near the surface[130], which certainly would not be noticeable in systems of the size considered here.

XI. SUPERCONDUCTIVITY AND CHARGE IMBALANCE

Within the BCS formalism, the total electronic charge per site is given by

$$Q_{tot} = \frac{2}{N} \sum_k [u_k^2 f(E_k) + v_k^2 (1 - f(E_k))] \quad (26)$$

in units of the charge of one carrier, e or $-e$ depending on whether one is using electron or hole representation.

Eq. (26) can be written as[131]

$$Q_{tot} = Q_c + Q^* \quad (27)$$

with

$$Q_c = \frac{2}{N} \sum_k v_k^2 \quad (28a)$$

the charge of the condensate, and

$$Q^* = \frac{2}{N} \sum_k (u_k^2 - v_k^2) f(E_k) \quad (28b)$$

the average charge of the quasiparticles. The coherence factors are given by the usual form

$$u_k^2 = \frac{1}{2} \left(1 + \frac{\epsilon_k - \mu}{E_k} \right) \quad (29a)$$

$$v_k^2 = \frac{1}{2} \left(1 - \frac{\epsilon_k - \mu}{E_k} \right). \quad (29b)$$

In a conventional BCS superconductor $Q^* = 0$ in equilibrium since quasiparticles are charge neutral on average, half electron, half hole. A non-zero Q^* , termed “charge imbalance” or “branch imbalance”, can be generated in a non-equilibrium situation in the presence of current flow[132, 133] and/or a temperature gradient[134, 135].

Instead, in the dynamic Hubbard model (or the correlated hopping model) a branch imbalance exists even in equilibrium[60]. The gap function has a slope of universal sign[55]

$$\Delta_k \equiv \Delta(\epsilon_k) = \Delta_m(-\epsilon_k/(D/2) + c) \quad (30)$$

with D the bandwidth and $\Delta_m > 0$ and c obtained from solution of the BCS equations[55]. The minimum gap is $\Delta_0 = \Delta(\mu)/a$, with $a = \sqrt{1 + (\Delta_m/(D/2))^2}$ and the quasiparticle energy is given by

$$E_k = \sqrt{a^2(\epsilon_k - \mu - \nu)^2 + \Delta_0^2}. \quad (31)$$

The minimum gap Δ_0 is attained not at $\epsilon_k = \mu$ but at $\epsilon_k = \mu + \nu$, with

$$\nu = \Delta_m(T)\Delta_0(T)/(aD/2) > 0. \quad (32)$$

Both Δ_0 and Δ_m go to zero at T_c as $\sqrt{T_c - T}$ so ν goes to zero linearly as T approaches T_c from below. The gap function and quasiparticle excitation spectrum are shown schematically in Figure 20 in hole representation. In equilibrium, quasiparticles are symmetrically distributed around the minimum located at $\epsilon_k^0 = \mu + \nu$ and as a consequence $Q^* > 0$, quasiparticles are positively charged on average. If we ignore band edge effects we have simply

$$Q^* = \frac{2\nu}{N} \sum_k \frac{f(E_k)}{E_k} \quad (33)$$

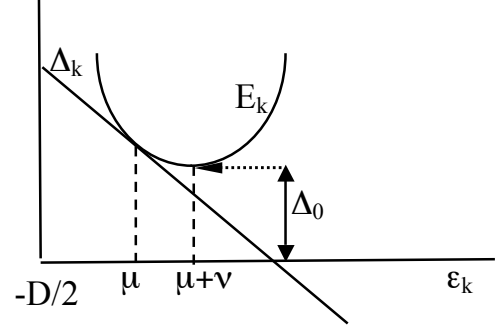


FIG. 20: Gap function Δ_k and quasiparticle energy E_k as a function of band energy ϵ_k in hole representation.

which is given approximately by (again ignoring band edge effects)

$$Q^* = \sqrt{8\pi} \frac{\nu(T)}{Da} \frac{e^{-\beta\Delta_0}}{(\beta\Delta_0)^{1/2}}, \quad (34)$$

Q^* is suppressed at low temperatures due to the exponential factor, peaks somewhat below T_c and goes to zero at T_c . Numerical examples are shown in ref. [60]. However when the finite bandwidth is taken into account Q^* remains positive at T_c and above.

Figure 21 shows the distribution as a function of the distance to the center r of the quasiparticle charge Q_i^* at site i , given by

$$Q_i^* = \frac{2}{N} \sum_n (u_{ni}^2 - v_{ni}^2) f(E_n) \quad (35)$$

obtained from solution of the BdG equations, for a dynamic Hubbard model and for an attractive Hubbard model. In Eq. (35), u_{ni} and v_{ni} are the amplitudes of the n -th eigenvector at site i obtained from diagonalization of the BdG Hamiltonian[103], E_n is the energy for state n and f is the Fermi function. In the attractive Hubbard model (Fig. 21 lower panel) particle-hole symmetry is broken only because the band is not half-full, but the interaction is particle-hole symmetric. As a consequence, the quasiparticle charge oscillates between positive and negative values. Instead, as seen in Fig. 21 (upper panel) in the dynamic Hubbard model quasiparticles are predominantly positively charged, as expected due to the shift in the chemical potential by ν displayed in Fig. 20.

Figure 22 shows the real space distribution of the quasiparticle charge in the dynamic Hubbard model (right panel). The total site occupation for this case is shown on the left panel. It can be seen from Figs. 20 and 21 that the positive quasiparticle charge is located mostly near the surface of the system. This is relevant to the discussion in the next section.

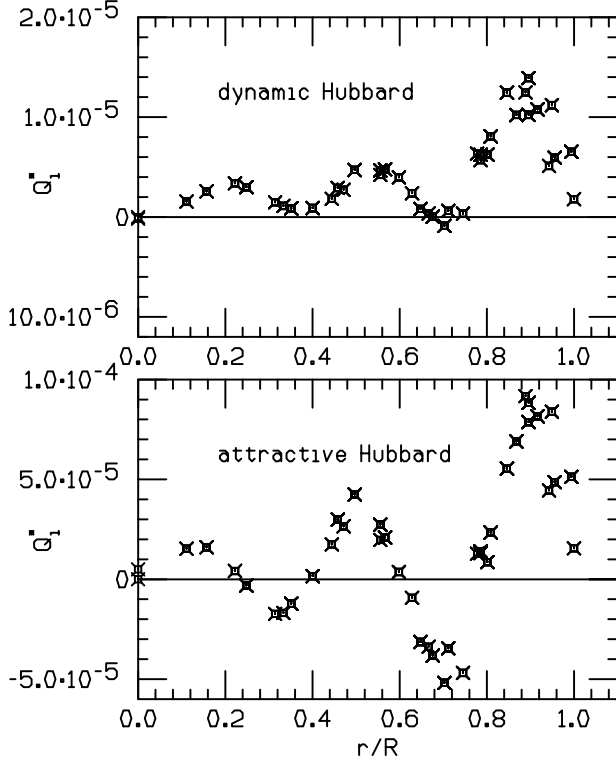


FIG. 21: Quasiparticle charge (Eq. (35)) as function of distance to the center for a dynamic Hubbard model with parameters as in Fig. 17 and for an attractive Hubbard model with $t_h = 0.1$, $U = -0.4$. Average occupation is $n = 0.126$, temperature is $k_B T = 0.01$. Note that in the dynamic Hubbard model the quasiparticle charge is predominantly positive.

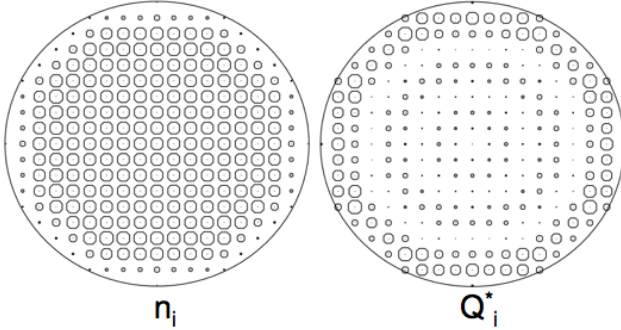


FIG. 22: Real space hole occupation (left panel) and quasiparticle charge (right panel) in the superconducting state of the dynamic Hubbard model. Parameters are the same as for Figure 21 (upper panel). Note that the quasiparticle charge is predominantly near the surface of the sample.

XII. TWO-FLUID MODEL AND INTERIOR ELECTRIC FIELD

In this section we discuss to what extent the dynamic Hubbard model reflects the physics shown in Figure 2 in the superconducting state, how it depends on tempera-

ture, and how this physics could be detected experimentally.

We assume a two-fluid model, with the total carrier concentration independent of temperature. We have then

$$n_s = n_s(T) + n_n(T) \quad (36)$$

with n_s the total carrier (hole) concentration and $n_s(T)$ and $n_n(T)$ the superfluid and normal components at $0 \leq T \leq T_c$. Within the two-fluid interpretation of BCS theory they are given in terms of the London penetration depth as

$$n_s(T) = n_s \frac{\lambda_L^2}{\lambda_L^2(T)} \quad (37a)$$

$$n_n(T) = n_s \lambda_L^2 \left(\frac{1}{\lambda_L^2} - \frac{1}{\lambda_L(T)^2} \right) \quad (37b)$$

with λ_L ($\lambda_L(T)$) the London penetration depths at zero (finite) temperature. Ignoring finite bandwidth effects the quasiparticle density is then [136]

$$n_n(T) = 2n_s \int_{\Delta_0}^{\infty} dE \left(-\frac{\partial f}{\partial E} \right) \frac{E}{\sqrt{E^2 - \Delta_0^2}} \quad (38)$$

which yields at low temperatures

$$n_n(T) = \sqrt{2\pi} (\beta \Delta_0)^{1/2} e^{-\beta \Delta_0} n_s. \quad (39)$$

On the other hand, the average quasiparticle charge per site is given by Eq. (34). Combining with Eq. (39),

$$\frac{Q^*(T)}{n_n(T)} = \frac{1}{a} \frac{k_B T}{D/2} \frac{\nu}{\Delta_0} = \frac{k_B T \Delta_m}{\Delta_m^2 + (D/2)^2} \sim \frac{k_B T \Delta_m}{(D/2)^2}. \quad (40)$$

It can be seen that the quasiparticle charge is a small fraction of the quasiparticle density. For example, for the parameters of Fig. 21 we have

$$D = 2z(t_h + n\Delta t + \frac{n^2}{4}\Delta t_2) = 1.01, \quad (41)$$

$\Delta_{ij} = 0.00253$, $\Delta_m = z\Delta_{ij} = 0.10$, hence $Q^*/n_n = 0.004$.

Assuming the system as a whole is charge neutral, the negative charge of the electrons in the band exactly compensates the positive charge of the ions, which is uniformly distributed in space (except for variations on the scale of \AA). At temperatures below T_c , the quasiparticles have a net positive charge, hence as a consequence the condensate has a total negative charge *greater* than the total positive charge of the ions. The condensate is highly mobile, and just like in a normal metal any excess negative charge will move to the surface [137] it is natural to expect that negative charge from the condensate will move to the surface.

Furthermore, we have seen in the previous section that the positive quasiparticle charge is located predominantly

near the surface in the superconducting state (Fig. 22 right panel). This can be interpreted as reflecting the fact that the superfluid has higher negative density near the surface, and the positive normal fluid consequently develops higher density near the surface to screen the superfluid charge. In addition, as already seen in the normal state of the dynamic Hubbard model, the total hole concentration is smaller near the surface which implies extra negative charge near the surface. Thus we argue that the dynamic Hubbard model provides support to the prediction of the electrodynamic equations of the theory[24, 25] that the superconductor expels superfluid negative charge from the interior to the surface.

Whether or not a macroscopic electric field will exist in the interior of the superconductor depends on whether there are enough quasiparticles to screen the electric field created by the negative charge expulsion of the condensate. In the ground state (no quasiparticles) the theory predicts that the net positive charge density in the interior is[130]

$$\rho_0 = \frac{r_q}{R} |e| n_s = \rho_s + \rho_{ions} \quad (42)$$

with R the radius of the cylinder and $r_q = \hbar/(2m_e c) = 0.00193\text{\AA}$ the quantum electron radius, and there is a negative charge density

$$\rho_- = -\frac{R}{2\lambda_L} \rho_0 = \rho_s + \rho_{ions} \quad (43)$$

within a London penetration depth of the surface, as shown schematically in Fig. 2. The charge densities at zero temperature are shown schematically in the left panels of Figure 23. ρ_s denotes the superfluid charge density.

At finite temperatures, there is a positive quasiparticle charge density excited, $\rho_n = |e|Q^*$, and a crossover temperature T_{cr} can be defined. For temperatures lower than T_{cr} , the average quasiparticle charge density excited is smaller than ρ_0 . In the middle top panel of Fig. 23 we assume ρ_n is uniformly distributed, and in the right top panel we assume all ρ_n has moved to within the London penetration depth of the surface. Even so, it is unable to screen the internal electric field, since a positive net charge density $\rho = \rho_0 - \rho_n > 0$ remains in the interior and a negative net charge density $\rho < 0$ remains near the surface, as shown in the top right panel of Fig. 23. At the crossover temperature T_{cr} the quasiparticle charge density excited reaches the value ρ_0 , and by migrating to the region within a London penetration depth of the surface (lower right panel of Fig. 23) it can completely screen both the interior positive charge and the negative charge in the surface layer, so that the electric field everywhere gets cancelled. This will also be the case at any temperature $T > T_{cr}$.

The value of the crossover temperature can be obtained from the equation

$$Q^* = \frac{Q^*}{n_n} n_n = \frac{r_q}{R} n_s \quad (44)$$

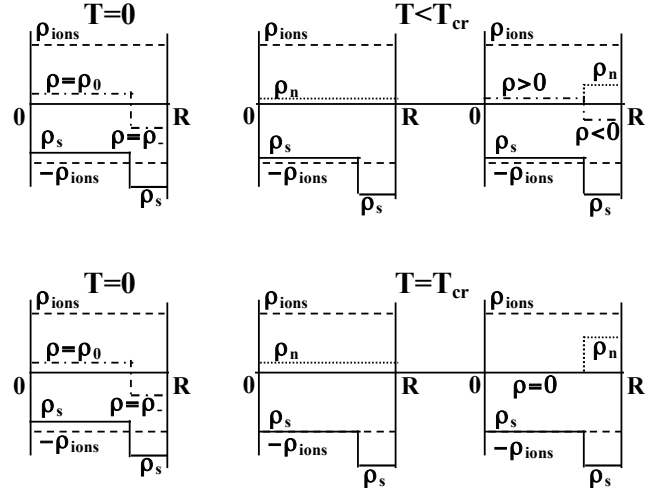


FIG. 23: Charge distribution in the superconductor (schematic). In the ground state (left panels) there is an excess positive charge density ρ_0 in the interior and an excess negative charge density ρ_- near the surface. At low temperatures $T < T_{cr}$ (upper panels) the charge density is partially screened by excited quasiparticles but a net positive charge density $\rho > 0$ remains in the interior and a net negative charge density $\rho < 0$ near the surface (dot-dashed lines in upper right panel). At temperature $T = T_{cr}$ and above the net charge density is zero both in the interior and near the surface.

with Q^*/n_n given by Eq. (40) and n_n given by Eq. (39), hence

$$\frac{k_B T_{cr} \Delta_m}{(D/2)^2} \left(\frac{2\pi \Delta_0}{k_B T_{cr}} \right)^{1/2} e^{-\Delta_0/(k_B T_{cr})} = \frac{r_q}{R}. \quad (45)$$

For example, assuming the usual relation $2\Delta_0/k_B T_c = 3.53$, for the case under consideration with $Q^*/n_n = 0.004$ and assuming $R = 500\text{nm}$ yields $T_{cr} = 0.16T_c$. For temperatures lower than T_{cr} , a nonzero electric field is predicted to exist in the interior of the superconductor.

In the presence of a non-zero internal electric field, superconductors of non-spherical shape should also develop electric fields extending to the region exterior to the body, of magnitude and direction determined by the shape of the body and the electrodynamic equations of the superconductor[128, 129]. These electric fields should be experimentally detectable in the neighborhood of superconductors at temperature lower than T_{cr} . In addition, the internal electric field should be directly detectable in electron holography experiments, as discussed in a recent paper[138]. The magnitude of these predicted electric fields is of order of H_{c1} , the lower critical magnetic field, in the interior of the superconductor[130], and an appreciable fraction of it in the region outside the superconductor near the surface, depending on the shape of the body[128, 129]. No external electric field is expected outside a planar surface or a spherical body.

XIII. THE MEISSNER EFFECT, THE LONDON MOMENT AND THE GYROMAGNETIC EFFECT

The fact that in superconductors the superfluid carries *negative charge* is established experimentally from experiments that measure the London moment[139, 140]: a rotating superconductor develops a magnetic field that is always *parallel*, never antiparallel, to the direction of the mechanical angular momentum of the body[59].

We have seen that the dynamic Hubbard model has a tendency to expel negative charge, that in a real system is inhibited in the normal state because of the effect of long-range Coulomb repulsion but may take place when the system becomes superconducting. The considerations in the previous section suggest that as a system becomes superconducting the electrons that condense into the superfluid state are partially expelled towards the surface, and at the same time normal electrons flow inward to compensate for the charge imbalance, as indicated by the fact that the positive quasiparticle charge moves outward in the superconducting state as seen in the last section.

Consider now these processes in the presence of an external magnetic field in the z direction, as shown in Fig. 24. The outflowing superfluid electrons will be deflected counterclockwise by the Lorentz force exerted by the magnetic field, building up a Meissner current flowing clockwise near the surface that suppresses the applied field in the interior. At the same time, the inflowing normal electrons are deflected clockwise by the magnetic field. Because these electrons undergo scattering from the ions, they will transmit their momentum to the ions and the body as a whole will start rotating in a clockwise direction. And because these electrons are slowed down and ultimately stopped by the collisions with the ions they will not reinforce the applied magnetic field. The end result is a superfluid current near the surface flowing in counterclockwise direction (i.e. superfluid electrons flowing in counterclockwise direction) that suppresses the interior magnetic field, and a slow body rotation in the clockwise direction that exactly cancels the mechanical angular momentum carried by the superfluid electrons in the Meissner current, as required by angular momentum conservation.

The magnetic field generated by rotating superconductors (London moment)[139, 140] can be similarly explained[141] by the fact that in a rotating normal metal that is cooled into the superconducting state the expelled superfluid electrons, that are moving at the same angular velocity as the body, will have a smaller tangential velocity than the body when they reach the surface, giving rise to a net current and resulting magnetic moment in direction *parallel*, never antiparallel, to the angular momentum of the rotating body.

More quantitatively, the outflow occurs because superfluid electrons expand their orbits from microscopic radius k_F^{-1} to mesoscopic radius $2\lambda_L$ [142], in the process

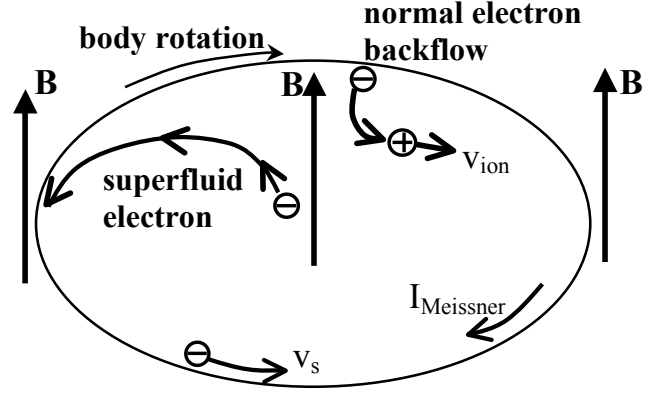


FIG. 24: The outflowing superfluid electrons are deflected in the counterclockwise direction by the applied magnetic field, generating a clockwise Meissner current ($I_{Meissner}$) near the surface that suppresses the magnetic field in the interior. The inflowing normal electrons collide with the ions and impart the entire body with angular momentum antiparallel to the applied magnetic field, that is equal and opposite to the mechanical angular momentum of the electrons in the Meissner current.

acquiring an azimuthal velocity[143]

$$v_\phi = -\frac{e}{2m_e c} r = -\frac{e}{m_e c} \lambda_L B \quad (46)$$

which is the speed of the superfluid electrons in the Meissner current[136]. The total mechanical angular momentum acquired by these electrons in a cylinder of radius R and height h is

$$L_{el} = \pi R^2 h n_s (m_e v_\phi 2\lambda_L) \quad (47)$$

which coincides with the total electronic angular momentum of the Meissner current flowing within a London penetration depth of the surface

$$L_{Meissner} = 2\pi R \lambda_L h n_s (m_e v_\phi R). \quad (48)$$

The inflowing normal electrons transmit the same angular momentum to the body as a whole by collisions with the ions, as required by angular momentum conservation[144]. As a consequence, the body starts rotating with angular velocity determined by the condition of angular momentum conservation, as measured experimentally[145–147] (gyromagnetic effect).

These processes provide an intuitive explanation for the dynamics of the Meissner effect[142], the generation of the London moment, the gyromagnetic effect and the puzzle of angular momentum conservation[144, 148] in superconductors, *provided* the superconductor is described by a dynamic Hubbard model that gives rise to negative charge expulsion. In superconductors not described by dynamic Hubbard models but by conventional BCS-electron-phonon theory[136] no charge expulsion takes place so these considerations don't apply. In those superconductors the dynamical origins of the

Meissner effect and the London moment and the explanation of the angular momentum puzzle remain to be elucidated.

XIV. DISCUSSION

Both the conventional Hubbard model and the dynamic Hubbard model are simplified descriptions of real materials, and whether or not they contain the physics of interest for particular real materials is in principle an open question. In this paper we have argued that the new physics that the dynamic Hubbard model incorporates beyond what is contained in the conventional Hubbard model has vast implications for the understanding of many materials of current interest.

The new physics of the dynamic Hubbard model is that it allows the electronic orbital to expand when it is doubly occupied. This expansion has associated with it outward motion of negative charge as well as lowering of the electron's kinetic energy *at the atomic level*, and it is of course not “electron-hole symmetric”. This physics is not included in the conventional Hubbard model that assumes that the electronic orbital is infinitely rigid. The key question is not whether this physics exists in real atoms, of course it does[3], the key questions are how large the effect is, what are its consequences, and under which conditions and for which materials is it or is it not relevant for various properties of the materials.

The mathematical treatment of the model is not simple, and from the outset we restricted ourselves in this paper to the antiadiabatic limit, i.e. assuming that the energy scale associated with the orbit expansion (ω_0 in Eq. (4)) is sufficiently large than it can be assumed infinite. This brings about the simplification that the high energy degrees of freedom can be eliminated and the Hamiltonian becomes equivalent to the low energy effective Hamiltonian Eq. (7), a Hubbard model with correlated hoppings, linear and nonlinear terms Δt and Δt_2 . This low energy effective Hamiltonian, together with the quasiparticle weight renormalization described by Eq. (6), describes many properties that we believe are relevant to real materials and are not described by the conventional Hubbard model. In particular it gives rise to hole superconductivity[55], driven by lowering of kinetic energy of the carriers[56, 149], with many characteristic features that resemble properties of the cuprates. In other work we have also examined the effect of the high energy degrees of freedom in describing spectral weight transfer from high to low energies (“undressing”[86]) as the number of holes increases and as the system enters the superconducting state, as well as the effect of finite ω_0 in further promoting pairing in this model[89].

In this paper we have shown with specific quantitative examples that the dynamic Hubbard model has a strong tendency to expel negative charge from the interior of the system to the surface, driven by lowering of kinetic energy of the charge carriers. We believe it is truly no-

table that this property of the model mimics the physics of the single atom that motivated the formulation of the model, *even though* the kinetic energy lowering and negative charge cloud expansion of the atomic electron is *not* explicitly included in the site Hamiltonian Eq. (1). It is furthermore notable that the orbital expansion in an ion is larger when the ion is negatively charged, which in the model translates to a larger value of the coupling constant g (smaller S , Eq. (6b)), larger $\Delta t/t_h$ (Eq. (10)) and consequently larger tendency for the model to expel negative charge. We argue that the fact that the lattice Hamiltonian Eq. (9) describes at a macroscopic length scale the same physics at the atomic scale that motivated the Hamiltonian is a strong indication that the Hamiltonian is relevant for the description of reality.

The tendency of the dynamic Hubbard model to expel negative charge and the tendency to pairing of holes and superconductivity of course go hand in hand: they both originate in the fact that the kinetic energy of a hole is lowered when another hole is nearby. Increasing the chance of having another hole nearby can be achieved by negative charge expulsion, thus increasing the *overall* hole density, and by pairing, thus increasing the *local* hole density.

The effects predicted by this Hamiltonian are largest when the coupling constant g is large, or equivalently when the overlap matrix element S is small, which corresponds to a “soft orbital” that would exist for negatively charged anions, *and* the effects are also largest when the band is almost full with negative electrons (strong coupling regime)[150]. Thus, not surprisingly, more negative charge at the ion or/and in the band yield larger tendency to negative charge expulsion for the entire system. We believe that the Hamiltonian is relevant to describe the physics of many superconductors of current interest including high T_c cuprates, *Fe* pnictides, *Fe* chalcogenides, *MgB₂* and *BiS₂*-based[151] superconductors. All these materials have negatively charged ions (O^{--} , As^{---} , S^{--} , Se^{--} , B^-) with soft orbitals, and for most of them, including “electron-doped” cuprates[152], there is experimental evidence for dominant *hole* transport in the normal state. We suggest that the orbital expansion and contraction of these negative ions depending on their electronic occupation is responsible for many interesting properties of these materials including their superconductivity, and is described by the dynamic Hubbard model.

In addition, we have seen in this paper that the model leads to charge inhomogeneity driven by lowering of kinetic energy, and in extreme cases to phase separation, and that it leads to negatively charged grain boundaries and depletion of hole carriers in the vicinity of grain boundaries, properties experimentally observed in many of these materials but not understood using conventional models such as “band bending”.

We have also examined here the question whether the interior[25] and exterior[128] electric fields predicted to exist in the ground state of superconductors within this

theory would exist also at finite temperatures and concluded that they should exist and hence be experimentally detectable up to a crossover temperature T_{cr} , calculated to be $0.16T_c$ in one example.

Finally, we have proposed that the negative charge expulsion predicted by dynamic Hubbard models is relevant to the understanding of the Meissner effect, the London moment and the gyromagnetic effect exhibited by superconductors that are not described by conventional BCS-electron phonon theory.

In summary, we hope the reader will appreciate the remarkable qualitative similarity of Figs. 1 and 2, depicting an atom and a superconductor within this model. Superconductors have been called “giant atoms” in the early days of superconductivity for many *other* reasons[153–155]. The essential property of the atom, that it is *not* electron-hole symmetric because the negative electron is much lighter than the positive nucleus, manifests itself identically in the atom described by the dynamic Hubbard model and in the state of a macroscopic superconducting body described by the model, and is missed in the world described by particle-hole symmetric conventional

Hubbard models both at the atomic level and at the level of the macroscopic superconductor. The superconductor is indeed a “giant atom” within our description, with the highly mobile light negative superfluid reflecting the nimble atomic electron, and the heavy positive quasiparticles reflecting the positive nucleus.

Much of the physics of dynamic Hubbard models for finite ω_0 remains to be understood. In fact, the model itself may require substantial modification to account for different values of ω_0 for different electronic occupations: the excitation spectrum of H is certainly very different from that of H^- . In connection with this and going beyond the antiadiabatic limit where only diagonal transitions of the auxiliary boson field are taken into account as in this paper, it is possible that *vertical* transitions may play a key role in describing the superconducting state[156]. It is also an open question to what extent dynamic Hubbard models can describe the mysterious “pseudogap state” of underdoped high T_c cuprate materials. These and other questions will be the subject of future work.

-
- [1] “The Hubbard Model: A Collection of Reprints”, ed. by A. Montorsi, World Scientific, Singapore, 1992.
 - [2] “The Hubbard model: its physics and mathematical physics”, ed. by D. Baeriswyl, D.K. Campbell, J.M.P. Carmelo, F. Guinea and E. Louis, NATO ASI Series B Vol. 343, Plenum, New York, 1995.
 - [3] J.C. Slater, *Quantum Theory of Atomic Structure*, McGraw-Hill, New York, 1960.
 - [4] J.E. Hirsch, Phys. Lett. A **134**, 451 (1989).
 - [5] A. Fortunelli and A. Painelli, Chem. Phys. Lett. **214**, 402 (1993).
 - [6] J.E. Hirsch, Physica B **199&200**, 366 (1994).
 - [7] G. H. Bach and F. Marsiglio, Jour. Sup. Nov. Mag. **24**, 1571 (2011).
 - [8] J.E. Hirsch and S. Tang, Sol. St. Comm. **69**, 987 (1989).
 - [9] J.E. Hirsch, Phys. Rev. B **43**, 11400 (1991).
 - [10] J.E. Hirsch, Physica C **201**, 347 (1992).
 - [11] J.E. Hirsch, Phys.Rev. Lett. **87**, 206402 (2001).
 - [12] P. Sun and G. Kotliar, Phys. Rev. B **66**, 085120 (2002).
 - [13] A.S. Moskvina and Y.D. Panov, Phys. Rev. B **68**, 125109 (2003).
 - [14] F. Aryasetiawan et al, Phys. Rev. B **70**, 195104 (2004).
 - [15] L. Arrachea and A.A. Aligia, Physica C **408**, 224 (2004).
 - [16] A. S. Moskvina, Low Temp. Phys. **33**, 234 (2007).
 - [17] K. Bouadim et al, Phys. Rev. B **77**, 014516 (2008).
 - [18] G. H. Bach, J.E. Hirsch and F. Marsiglio, Phys. Rev. B **82**, 155122 (2010).
 - [19] G. H. Bach and F. Marsiglio, Phys. Rev. B **85**, 155134 (2012).
 - [20] M. Casula et al, Phys. Rev. Lett. **109**, 126408 (2012).
 - [21] J.E. Hirsch, Phys.Rev. B **65**, 184502 (2002).
 - [22] P. Pincus, Solid St. Comm. **11**, 51 (1972).
 - [23] J.E. Hirsch, Phys. Lett. A **168**, 305 (1992).
 - [24] J.E. Hirsch, Phys. Lett. A **281**, 44 (2001).
 - [25] J.E. Hirsch, Phys.Rev. B **68**, 184502 (2003); Phys.Rev. B **69**, 214515 (2004).
 - [26] J.E. Hirsch and F. Marsiglio, Physica C **331**, 150 (2000).
 - [27] V. J. Emery and S. A. Kivelson, Jour. Phys. Chem. Solids **61**, 467 (2000).
 - [28] S. Chakravarty, Hae-Young Kee and E. Abrahams, Phys. Rev. B **67**, 100504 (2003).
 - [29] E. W. Carlson, V. J. Emery, S. A. Kivelson and D. Orgad, in “Superconductivity: Conventional and Unconventional Superconductors”, ed. by K. H. Bennemann and John B. Ketterson, Springer, Berlin, 2008, p. 1225–1348.
 - [30] M. R. Norman, M. Randeria, B. Jank and J. C. Campuzano, Phys. Rev. B **61**, 14742 (2000).
 - [31] P. Wrobel, R. Eder and R. Micnas, J. Phys. Condens. Matter **15**, 2755 (2003).
 - [32] T. Eckl, W. Hanke and E. Arrigoni, Phys. Rev. B **68**, 014505 (2003).
 - [33] R. Haslinger and A. V. Chubukov, Phys. Rev. B **68**, 214508 (2003).
 - [34] S. Feng, Phys. Rev. B **68**, 184501 (2003).
 - [35] M. Ogata, H.Yokoyama, Y. Yanase, Y. Tanaka and H.Tsuchiura, Jour. Phys. Chem. Solids **67**, 37 (2006).
 - [36] Th. A. Maier, M. Jarrell, A. Macridin and C. Slezak, Phys. Rev. Lett. **92**, 027005 (2004).
 - [37] Z. C. Gu, Tao Li, and Z. Y. Weng, Phys. Rev. B **71**, 064502 (2005).
 - [38] B. Kyung, A. Georges and A.-M. S. Tremblay, Phys. Rev. B **74**, 024501 (2006).
 - [39] J.P. Carbotte and E. Schachinger, J. Low Temp. Phys. **144**, 61 (2006).
 - [40] K. Haule and G. Kotliar, Europhysics Letters **77**, 27007 (2007).
 - [41] M. R. Norman, A. V. Chubukov, E. van Heumen, A. B. Kuzmenko, and D. van der Marel, Phys. Rev. B **76**,

- 220509(R) (2007)
- [42] Saurabh Maiti and Andrey V. Chubukov, Phys. Rev. B **81**, 245111 (2010)
- [43] L. Vidmar and J. Bonca, Phys. Rev. B **82**, 125121 (2010).
- [44] D. van der Marel, H.J.A. Molegraaf, C. Presura and I. Santos, in “Concepts in electron correlation”, ed. by A. Hewson and V. Zlatić, Kluwer, Dordrecht, (2003), arXiv:cond-mat/0302169 (2003).
- [45] H.L. Dewing and E.K.H. Salje, Supercond. Sci. Technol. **5**, 50 (1992).
- [46] L. Fugol, V. Samoyarov, A. Ratner and V. Zhuravlev, Solid St. Comm. **86**, 385 (1993); Physica C **216**, 391 (1993).
- [47] D.N. Basov et al, Science **283**, 49 (1999).
- [48] H. J. A. Molegraaf, C. Presura, D. van der Marel, P. H. Kes, and M. Li Science **295**, 2239 (2002).
- [49] A. F. Santander-Syro, R. P. Lobo, N. Bontemps, Z. Konstantinovic, Z. Z. Li and H. Raffy, Europhys. Lett., **62** 568 (2003).
- [50] F. Carbone, A. B. Kuzmenko, H. J. A. Molegraaf, E. van Heumen, E. Giannini, and D. van der Marel, Phys. Rev. B **74**, 024502 (2006)
- [51] F. Carbone et al, Phys. Rev. B **74**, 064510 (2006).
- [52] G. Deutscher, A. F. Santander-Syro, and N. Bontemps, Phys. Rev. B **72**, 092504 (2005).
- [53] A. Charnukha, P. Popovich, Y. Matiks, D. L. Sun, C. T. Lin, A. N. Yaresko, B. Keimer, A. V. Boris, arXiv:1009.5915 (2010).
- [54] C. Giannetti et al, Nature Comm. **2**, 353 (2011).
- [55] J.E. Hirsch and F. Marsiglio, Phys. Rev. B **39**, 11515 (1989); Phys. Rev. B **48**, 4807 (1992); F. Marsiglio and J.E. Hirsch, Phys. Rev. B **41**, 6435 (1990).
- [56] J.E. Hirsch, Physica C **199**, 305 (1992).
- [57] J.E. Hirsch and F. Marsiglio, Phys. Rev. B **62**, 15131 (2000).
- [58] F. Marsiglio, Jour. Sup. Nov. Mag. **22**, 269 (2009).
- [59] J.E. Hirsch, Phys. Rev. B **68**, 012510 (2003).
- [60] J.E. Hirsch, Phys. Rev. Lett. **72**, 558 (1994).
- [61] A. Bianconi et al, Jour. of Phys. Cond. Matt. **12**, 10655 (2000).
- [62] S.A. Kivelson et al, Rev. Mod. Phys. **75**, 1201 (2003).
- [63] E. Dagotto, Science **309**, 257 (2005).
- [64] S.H. Pan et al, Nature **413**, 282 (2001).
- [65] Y. Kohsaka et al, Nature Physics **8**, 534 (2012).
- [66] J. Bardeen, Phys. Rev. **97**, 1724 (1955).
- [67] T. Matsubara, Prog. Theor. Phys. **13**, 631 (1955).
- [68] J. Bardeen, L. N. Cooper, and J. R. Schrieffer, Phys. Rev. **108**, 1175 (1957).
- [69] P. W. Anderson, Phys. Rev. **110**, 827 (1958).
- [70] G. Rickayzen, Phys. Rev. **111**, 817 (1958); Phys. Rev. Lett. **2**, 90 (1959); Phys. Rev. **115**, 795 (1959).
- [71] G. Wentzel, Phys. Rev. **111**, 1488 (1958); Phys. Rev. Lett. **2**, 33 (1959).
- [72] D. Pines and J. R. Schrieffer, Phys. Rev. Lett. **1**, 407 (1958).
- [73] R.M. May and M.R. Schafroth, Phys. Rev. **115**, 1446 (1959).
- [74] Y. Nambu, Phys. Rev. **117**, 648 (1960).
- [75] L.P. Kadanoff and P.C. Martin, Phys. Rev. **124**, 670 (1961).
- [76] D.A. Uhlenbrock and B. Zumino, Phys. Rev. **133**, A350 (1964).
- [77] M.L. Cohen, Mod. Phys. Lett. B **24**, 2755 (2010).
- [78] M.R. Norman, Science **322**, 196 (2011).
- [79] J.E. Hirsch, Jour. Sup. Nov. Mag. **309**, 23 (2010).
- [80] J.E. Hirsch, Physica Scripta **85**, 035704 (2012).
- [81] W.A. Newcomb, Ann. Phys. **3**, 347 (1958).
- [82] J.E. Hirsch, Phys. Rev. B **67**, 035103 (2003).
- [83] J.E. Hirsch, Phys. Rev. B **47**, 5351.
- [84] J.E. Hirsch, Phys. Rev. B **62**, 14487 (2000).
- [85] J.D. Mahan, “Many Particle Physics”, Third Edition, Plenum, New York, 2000.
- [86] J.E. Hirsch, Phys. Rev. B **62**, 14487 (2000); Phys. Rev. B **62**, 14998 (2000).
- [87] J.E. Hirsch, Physica C **364-365**, 37 (2001).
- [88] J.E. Hirsch, Phys. Rev. B **65**, 214510 (2002); Phys. Rev. B **66**, 064507(2002).
- [89] F. Marsiglio, R. Teshima and J. E. Hirsch, Phys. Rev. B **68**, 224507 (2003).
- [90] S. Kivelson, W.-P. Su, J. R. Schrieffer, and A. J. Heeger, Phys. Rev. Lett. **58**, 1899 (1987).
- [91] D. K. Campbell, J. Tinka Gammel, and E. Y. Loh Phys. Rev. B **38**, 12043 (1988)
- [92] J.E. Hirsch and F. Marsiglio, Physica C **162-164**, 591 (1989).
- [93] G. Kotliar et al, Rev. Mod. Phys. **78**, 865 (2006).
- [94] R. Micnas, J. Ranninger and S. Robaszkiewicz, Rev. Mod. Phys. **62**, 113 (1990).
- [95] R.Z. Bariev et al, Jour. Phys. A **26**, 1249 (1993).
- [96] L. Arrachea et al, Phys. Rev. B **50**, 16044 (1994).
- [97] M. Airolidi and A. Parola, Phys. Rev. B **51**, 16327 (1995).
- [98] F. Marsiglio and J.E. Hirsch, Physica C **159**, 157 (1989).
- [99] J.E. Hirsch, Phys. Lett. A **309**, 457 (2003).
- [100] J.E. Hirsch, Physica C **478**, 42 (2012).
- [101] A. Montorsi, Jour. Stat. Mech. (2008) L09001.
- [102] A. Anfossi, C. D. E. Boschi and A. Montorsi, Phys. Rev. B **68**, 224507 (2003).
- [103] J.E. Hirsch, Physica C **194**, 119 (1992).
- [104] S.E. Babcock and J.L. Vargas, Ann. Rev. Mat. Sci **25**, 193 (1995).
- [105] H. Hilgenkamp and J. Mannhart, Rev. Mod. Phys. **74**, 485 (2002).
- [106] J. Mannhart, in ‘Thin Films and Heterostructures for Oxide Electronics’, Springer, 2005, p. 251.
- [107] S.E. Babcock et al, Physica C **227**, 183 (1994).
- [108] N.D. Browning et al, Physica C **212**, 185 (1993).
- [109] C.W. Schneider et al, Phys. Rev. Lett. **92**, 257003 (2004).
- [110] A. Schmehl et al, Europhys. Lett. **47**, 110 (1999).
- [111] G. Hammerl et al, Nature **407**, 162 (2000).
- [112] G.A. Daniels, A. Gurevich and D.C. Larbalestier, Appl. Phys. Lett. **77**, 3251 (2000).
- [113] J. Mannhart and H. Hilgenkamp, Supercond. Sci. Technol. **10**, 880 (1997).
- [114] A. Gurevich and E.A. Pashitskii, Phys. Rev. B **57**, 13878 (1998).
- [115] U. Schwingenschlogl and C. Schuster, EPL **77**, 37007 (2007).
- [116] V. Ravikumar, R.P. Rodrigues and V.P. Dravid, Phys. Rev. Lett. **75**, 4063 (1995).
- [117] M.A. Schofield, L. Wu and Y. Zhu, Phys. Rev. B **67**, 224512 (2003).
- [118] M.A. Schofield et al, Phys. Rev. Lett. **92**, 195502 (2004).
- [119] Ch. Joos et al, Physica C **408-410**, 443 (2004).
- [120] V. Ravikumar, R.P. Rodrigues and V.P. Dravid, Phys. Rev. Lett. **75**, 4063 (1995).

- [121] R.F. Klie et al, Nature **435**, 475 (2005).
- [122] C.T. Koch, Int. J. Mat. Res. **101**, 1 (2010).
- [123] S. H. Mennema et al, Phys. Rev. B **71**, 094509 (2005).
- [124] J.H. Durrell et al, Reports of Progress in Physics **74**, 124511 (2011) and references therein.
- [125] F. Marsiglio and J.E. Hirsch, Physica C **468**, 1047 (2008).
- [126] K. Kumagai, K. Nozaki and Y. Matsuda, Phys. Rev. B **63**, 144502 (2001).
- [127] V.F. Mitrovic et al, Phys. Rev. B **67**, 220503 (2003).
- [128] J.E. Hirsch, Phys.Rev. Lett. **92**, 016402 (2004).
- [129] J.E. Hirsch, Jour. Supercond. Novel Mag. **25**, 1357 (2012).
- [130] J.E. Hirsch, Ann. der Physik (Berlin) **17**, 380 (2008).
- [131] A.M. Kadin, L.N. Smith and W. J. Skocpol, J. Low Temp. Phys. **38**, 497 (1980).
- [132] J. Clarke, Phys. Rev. Lett. **28**, 1363 (1972).
- [133] M. Tinkham and J. Clarke, Phys. Rev. Lett. **28**, 640 (1979).
- [134] C. Pethick and H. Smith, Phys. Rev. Lett. **43**, 1366 (1972).
- [135] J. Clarke and M. Tinkham, , Phys. Rev. Lett. **44**, 106 (1980).
- [136] M. Tinkham, "Introduction to Superconductivity", 2nd ed, McGraw Hill, New York, 1996.
- [137] Y. Levin and J.J. Arenzon, Europhys. Lett. **63**, 415 (2003).
- [138] J.E. Hirsch, arXiv:1301.4999 (2013).
- [139] A.F. Hildebrand, Phys. Rev. Lett. **8**, 190 (1964).
- [140] A.A. Verheijen et al, Nature **345**, 418 (1990).
- [141] J.E. Hirsch, Phys. Rev. B **71**, 184521 (2005).
- [142] J.E. Hirsch, Europhys. Lett. **81**, 67003 (2008).
- [143] J.E. Hirsch, Jour. Sup. Nov. Mag. **22**, 131 (2009).
- [144] J.E. Hirsch, Phys. Lett. A **366**, 615 (2007).
- [145] I.K. Kikoin, S.W. Gubar, J. Phys. USSR **3**, 333 (1940).
- [146] R.H. Pry, A.L. Lathrop, W.V. Houston, Phys. Rev. **86**, 905 (1952).
- [147] R. Doll, Z. Phys. **153** (1958) 207
- [148] J.E. Hirsch, Jour. Phys. Cond. Matt. **20**, 235233 (2008).
- [149] J.E. Hirsch, Physica C **341-346**, 213 (2000).
- [150] F. Marsiglio and J.E. Hirsch, Physica C **165**, 71 (1990).
- [151] Y. Mizuguchi et al, J. Phys. Soc. Jpn. **81**, 114725 (2012).
- [152] W. Jiang et al, Phys. Rev. Lett. **73**, 1291 (1994); P. Fournier et al , Phys. Rev. B **56**, 14149 (1997); Y. Dagan and R.L. Greene, Phys. Rev. B **76**, 024506 (2007).
- [153] F. London and H. London, Physica **2**, 341 (1935).
- [154] H.G. Smith and J.O. Wilhelm, Rev. Mod. Phys. **4**, 237 (1935).
- [155] W. L. Ginsburg and H. Vogel, Fortschritte der Physik **1**, 101 (1953).
- [156] J.E. Hirsch, Int. J. Mod. Phys. **23**, 3035 (2009).